

# THE RELATIONSHIP BETWEEN STELLAR POPULATIONS AND Ly $\alpha$ EMISSION IN LYMAN BREAK GALAXIES<sup>1</sup>

KATHERINE A. KORNEI AND ALICE E. SHAPLEY<sup>2,3</sup>

Department of Physics and Astronomy, 430 Portola Plaza, University of California at Los Angeles, Los Angeles, CA 90025, USA

DAWN K. ERB<sup>4</sup>

Department of Physics, University of California at Santa Barbara, Santa Barbara, CA 93106, USA

CHARLES C. STEIDEL

California Institute of Technology, MS 105-24, Pasadena, CA 91125, USA

NAVEEN A. REDDY<sup>5</sup>

National Optical Astronomy Observatory, 950 N. Cherry Ave, Tucson, AZ 85719, USA

MAX PETTINI

Institute of Astronomy, Madingley Road, Cambridge, CB3 0HA, UK

MILAN BOGOSAVLJEVIĆ

California Institute of Technology, MS 105-24, Pasadena, CA 91125, USA

*Draft version February 7, 2020*

## ABSTRACT

We present the results of a photometric and spectroscopic survey of 321 Lyman break galaxies (LBGs) at  $z \sim 3$  to investigate systematically the relationship between Ly $\alpha$  emission and stellar populations. Ly $\alpha$  equivalent widths ( $W_{\text{Ly}\alpha}$ ) were calculated from rest-frame UV spectroscopy and optical/near-infrared/*Spitzer* photometry was used in population synthesis modeling to derive the key properties of age, dust extinction, star formation rate (SFR), and stellar mass. We directly compare the stellar populations of LBGs with and without strong Ly $\alpha$  emission, where we designate the former group ( $W_{\text{Ly}\alpha} \geq 20 \text{ \AA}$ ) as Ly $\alpha$ -emitters (LAEs) and the latter group ( $W_{\text{Ly}\alpha} < 20 \text{ \AA}$ ) as non-LAEs. This controlled method of comparing objects from the same UV luminosity distribution represents an improvement over previous studies in which the stellar populations of LBGs and narrowband-selected LAEs were contrasted, where the latter were often intrinsically fainter in broadband filters by an order of magnitude simply due to different selection criteria. Using a variety of statistical tests, we find that Ly $\alpha$  equivalent width and age, SFR, and dust extinction, respectively, are significantly correlated in the sense that objects with strong Ly $\alpha$  emission also tend to be older, lower in star formation rate, and less dusty than objects with weak Ly $\alpha$  emission, or the line in absorption. We accordingly conclude that, within the LBG sample, objects with strong Ly $\alpha$  emission represent a later stage of galaxy evolution in which supernovae-induced outflows have reduced the dust covering fraction. We also examined the hypothesis that the attenuation of Ly $\alpha$  photons is lower than that of the continuum, as proposed by some, but found no evidence to support this picture.

*Subject headings:* galaxies: high-redshift — galaxies: evolution — galaxies: starburst

## 1. INTRODUCTION

An increasing number of high-redshift galaxies have been found in the last two decades using selection techniques reliant on either color cuts around the Lyman limit at 912  $\text{\AA}$  in the rest frame (e.g., Steidel et al. 1996, 1999) or strong Ly $\alpha$  line emission (e.g., Cowie & Hu

1998; Rhoads et al. 2000; Gawiser et al. 2006). These two methods, which preferentially select Lyman break galaxies (LBGs) and Ly $\alpha$ -emitters (LAEs), respectively, have successfully isolated galaxies at redshifts up to  $z = 7$  (Iye et al. 2006; Bouwens et al. 2008). Extensive data sets of LBGs and LAEs have afforded detailed studies of galactic clustering (e.g., Adelberger et al. 1998; Giavalisco & Dickinson 2001), the universal star formation history (e.g., Madau et al. 1996; Steidel et al. 1999), and the galaxy luminosity function (e.g., Reddy et al. 2008; McLure et al. 2009). While the nature of LBGs and LAEs have been studied at a range of redshifts (e.g., Shapley et al. 2001; Gawiser et al. 2006; Verma et al. 2007; Pentericci et al. 2007; Nilsson et al. 2008; Ouchi

<sup>1</sup> Based, in part, on data obtained at the W.M. Keck Observatory, which is operated as a scientific partnership among the California Institute of Technology, the University of California, and NASA, and was made possible by the generous financial support of the W.M. Keck Foundation.

<sup>2</sup> Packard Fellow.

<sup>3</sup> Alfred P. Sloan Fellow.

<sup>4</sup> Spitzer Fellow.

<sup>5</sup> Hubble Fellow.

et al. 2008; Finkelstein et al. 2009), the epoch around  $z \sim 3$  is particularly well-suited to investigation of these objects' detailed physical properties. At this redshift, the prominent HI Ly $\alpha$  line ( $\lambda_{\text{rest}} = 1216 \text{ \AA}$ ), present in all LAE spectra and a significant fraction of LBG spectra, is shifted into the optical, where current imaging and spectroscopic instrumentation is optimized. Consequently, there are large existing data sets of spectroscopically-confirmed  $z \sim 3$  LBGs (e.g., Steidel et al. 2003) and LAEs (e.g., Lai et al. 2008), where extensive multiwavelength surveys often complement the former and, less frequently, the latter.

The mechanism responsible for LAEs' large Ly $\alpha$  equivalent widths is not fully understood, although several physical pictures have been proposed. As Ly $\alpha$  emission is easily quenched by dust, one explanation for LAEs is that they are young, chemically pristine galaxies experiencing their initial bursts of star formation (e.g., Hu & McMahon 1996; Nilsson et al. 2007). Conversely, LAEs have also been proposed to be older, more evolved galaxies with interstellar media in which dust is segregated to lie in clumps of neutral hydrogen surrounded by a tenuous, ionized dust-free medium (Neufeld 1991; Hansen & Oh 2006; Finkelstein et al. 2009). In this picture, Ly $\alpha$  photons are resonantly scattered near the surface of these dusty clouds and rarely encounter dust grains. Continuum photons, on the other hand, readily penetrate through the dusty clouds and are accordingly scattered or absorbed. This scenario preferentially attenuates continuum photons and enables resonant Ly $\alpha$  photons to escape relatively unimpeded, producing a larger Ly $\alpha$  equivalent width than expected given the underlying stellar population. To date, the distribution of dust in the interstellar medium has only been investigated using relatively small samples (e.g., Verhamme et al. 2008; Atek et al. 2009; Finkelstein et al. 2009).

Given the different selection techniques used to isolate LBGs and LAEs, understanding the relationship between the stellar populations of these objects has been an important goal of extragalactic research. Recent work by Gawiser et al. (2006) has suggested that LAEs are less massive and less dusty than LBGs, prompting these authors to propose that LAEs may represent the beginning of an evolutionary sequence in which galaxies increase in mass and dust content through successive mergers and star formation episodes (Gawiser et al. 2007). The high specific star formation rate – defined as star formation rate (SFR) per unit mass – of LAEs ( $\sim 7 \times 10^{-9} \text{ yr}^{-1}$ ; Lai et al. 2008) relative to LBGs ( $\sim 3 \times 10^{-9} \text{ yr}^{-1}$ ; Shapley et al. 2001) illustrates that LAEs are building up stellar mass at a rate exceeding that of continuum-selected galaxies at  $z \sim 3$ . This rapid growth in mass is consistent with the idea that LAEs represent the beginning of an evolutionary sequence of galaxy formation. However, results from Finkelstein et al. (2009) cast doubt on this simple picture of LAEs as primordial objects, given that these authors find a range of dust extinctions ( $A_{1200} = 0.30\text{--}4.50$ ) in a sample of 7 LAEs at  $z \sim 4.5$ . Nilsson et al. (2008) also find that  $z \sim 2.25$  LAEs occupy a wide swath of color space, additional evidence that not all LAEs are young, dust-free objects. Furthermore, the assertion that LAEs are pristine galaxies undergoing their first burst of star formation is called into question by the results of Lai et al. (2008). These authors present a sample of 70

$z \sim 3.1$  LAEs,  $\sim 30\%$  of which are detected in the  $3.6 \mu\text{m}$  band of the *Spitzer* Infrared Array Camera (IRAC; Fazio et al. 2004). These IRAC-detected LAEs are significantly older and more massive ( $\langle t_{\star} \rangle \sim 1.6 \text{ Gyr}$ ,  $\langle M \rangle \sim 9 \times 10^9$ ) than the IRAC-undetected sample ( $\langle t_{\star} \rangle \sim 200 \text{ Myr}$ ,  $\langle M \rangle \sim 3 \times 10^8 M_{\odot}$ ); Lai et al. (2008) suggest that the IRAC-detected LAEs may therefore be a lower-mass extension of the LBG population. Narrowband-selected LAEs are clearly marked by heterogeneity, and the relationship between these objects and LBGs continues to motivate new studies.

When comparing the stellar populations of LBGs and LAEs, it is important to take into account the selection biases that result from isolating these objects with broadband color cuts and line flux/equivalent width requirements, respectively. By virtue of selection techniques that rely on broadband fluxes and colors, LBGs generally have brighter continua than LAEs. Spectroscopic samples of LBGs typically have an apparent magnitude limit of  $\mathcal{R} \leq 25.5$  ( $0.4L^*$  at  $z \sim 3$ ; Steidel et al. 2003) while LAEs have a median apparent magnitude of  $R \sim 27$  (Gawiser et al. 2006), where  $\mathcal{R}$  and  $R$  magnitudes are comparable. Even though the majority of LBGs studied to date are an order of magnitude more luminous in the continuum than typical LAEs, both populations have similar rest-frame UV colors (Gronwall et al. 2007). Therefore, LAEs fainter than  $\mathcal{R} = 25.5$  are excluded from LBG spectroscopic surveys not because of their colors, but rather because of their continuum faintness. Given the significant discrepancy in absolute magnitude between LBGs and LAEs, understanding the relationship between these objects can be fraught with bias. A preferable approach to comparing these populations is to investigate how the strength of Ly $\alpha$  emission is correlated with galaxy parameters, for a controlled sample of objects at similar redshifts *drawn from the same parent UV luminosity distribution*.

Several authors have looked at the question of the origin of Ly $\alpha$  emission in UV flux-limited samples (e.g., Shapley et al. 2001; Erb et al. 2006a; Reddy et al. 2008; Pentericci et al. 2007; Verma et al. 2007). Shapley et al. (2001) analyzed 74 LBGs at  $z \sim 3$  and constructed rest-frame UV composite spectra from two samples of “young” ( $t_{\star} \leq 35 \text{ Myr}$ ) and “old” ( $t_{\star} \geq 1 \text{ Gyr}$ ) galaxies, respectively. These authors found that younger objects exhibited weaker Ly $\alpha$  emission than older galaxies; Shapley et al. (2001) attributed the difference in emission strength to younger LBGs being significantly dustier than their more evolved counterparts. On the other hand, Erb et al. (2006a) examined a sample of 87 star-forming galaxies at  $z \sim 2$  and found that objects with lower stellar mass had stronger Ly $\alpha$  emission features, on average, than more massive objects. In a sample of 139 UV-selected galaxies at  $z \sim 2\text{--}3$ , Reddy et al. (2008) isolated 14 objects with Ly $\alpha$  equivalent widths  $\geq 20 \text{ \AA}$  and noted no significant difference in the stellar populations of strong Ly $\alpha$ -emitters relative to the rest of the sample. Pentericci et al. (2007) examined 47 LBGs at  $z \sim 4$  and found that younger galaxies generally showed Ly $\alpha$  in emission while Ly $\alpha$  in absorption was associated with older galaxies (in contrast to the Shapley et al. (2003) results). Probing even earlier epochs, Verma et al. (2007) examined a sample of 21 LBGs at  $z \sim 5$  and found no

correlation between Ly $\alpha$  equivalent width and age, stellar mass, or SFR. These authors noted, however, that only 6/21 of the brightest LBGs had corresponding spectroscopy from which equivalent widths were estimated. Therefore, the lack of a correlation between Ly $\alpha$  equivalent width and stellar populations may, in this case, have been masked by a small sample that was biased towards the brightest objects. These aforementioned investigations have shown that there does not yet exist a clear picture relating stellar populations to Ly $\alpha$  emission.

In this paper, we present a precise, systematic investigation of the relationship between Ly $\alpha$  emission and stellar populations using our large photometric and spectroscopic data set of  $z \sim 3$  observations. As an improvement over previous studies, we approach the data analysis from multiple aspects: we compare not only the stellar population parameters derived from population synthesis modeling, but also examine the objects' best-fit SEDs and photometry. Furthermore, all analysis is conducted on objects drawn from the same parent sample of continuum-bright ( $\mathcal{R} \leq 25.5$ ) LBGs. By controlling for continuum magnitude, we avoid the biases of comparing objects with significantly different luminosities while still retaining the ability to comment on the nature of strong Ly $\alpha$ -emitting galaxies within the LBG sample. Our conclusions are applicable to both LBGs and bright ( $\mathcal{R} \leq 25.5$ ) narrowband-selected LAEs. While we are unable to make inferences about the population of faint LAEs, our study is complete with respect to bright LAEs given these objects' similar colors to LBGs in the rest-frame UV.

We are motivated by the following questions: how do the stellar populations of Ly $\alpha$ -emitting LBGs differ from those of other LBGs at  $z \sim 3$  where the Ly $\alpha$  emission line is weaker (or absent altogether)? To what degree are galactic parameters such as dust extinction, SFR, age, and stellar mass correlated with Ly $\alpha$  line strength? What do the relative escape fractions of Ly $\alpha$  and continuum photons reveal about the distributions of gas and dust in these objects' interstellar media?

This paper is organized as follows. In §2, we present details of the observations and data reduction, including a description of the systematic technique used to calculate Ly $\alpha$  equivalent widths. Stellar population modeling is discussed in §3. The properties of objects with and without strong Ly $\alpha$  emission are presented in §4 and we discuss how our data can be used to address several of the outstanding questions pertaining to the physical nature of LBGs and LAEs in §5. A summary and our conclusions appear in §6. We assume a standard  $\Lambda$ CDM cosmology throughout with  $H_0 = 70 \text{ km s}^{-1} \text{ Mpc}^{-1}$ ,  $\Omega_M = 0.3$ , and  $\Omega_\Lambda = 0.7$ . All magnitudes are based on the AB system (Oke & Gunn 1983)<sup>6</sup>, with the exception of the infrared passbands which are in the Vega system.

## 2. OBSERVATIONS AND DATA REDUCTION

### 2.1. Imaging and Spectroscopy

The data presented here are drawn from the LBG surveys of Steidel and collaborators, with approximately

<sup>6</sup> AB magnitude and  $f_\nu$ , the flux density in units of  $\text{ergs s}^{-1} \text{ cm}^{-2} \text{ Hz}^{-1}$ , are related by  $m_{\text{AB}} = -2.5 \log_{10} f_\nu - 48.6$ . Conversions between AB and Vega magnitudes for the near-infrared passbands are as follows:  $K_s(\text{AB}) = K_s(\text{Vega}) + 1.82$ ;  $J(\text{AB}) = J(\text{Vega}) + 0.90$ .

TABLE 1  
SPECTROSCOPIC SURVEY FIELDS

Field Name	$\alpha^a$ (J2000.0)	$\delta^b$ (J2000.0)	Field Size (arcmin <sup>2</sup> )	$N_{\text{LBG}}^c$
Q0100*	01 03 11	13 16 18	42.9	22
Q0142	01 45 17	-09 45 09	40.1	20
Q0449	04 52 14	-16 40 12	32.1	13
Q1009*	10 11 54	29 41 34	38.3	30
Q1217	12 19 31	49 40 50	35.3	13
GOODS-N <sup>d*</sup> †	12 36 51	62 13 14	155.3	54
Q1307	13 07 45	29 12 51	258.7	8
Q1549*†	15 51 52	19 11 03	37.3	48
Q1623*†	16 25 45	26 47 23	290.0	24
Q1700*†	17 01 01	06 11 58	235.3	39
Q2206*	22 08 53	-19 44 10	40.5	23
Q2343*†	23 46 05	12 49 12	212.8	26
Q2346	23 48 23	00 27 15	280.3	1
<b>TOTAL</b>	...	...	<b>1698.9</b>	<b>321</b>

<sup>a</sup>Right ascension in hours, minutes, and seconds.

<sup>b</sup>Declination in degrees, arcminutes, and arcseconds.

<sup>c</sup>Number of spectroscopically-confirmed LBGs with redshifts  $z \geq 2.7$ , excluding QSOs and AGN.

<sup>d</sup>This field is also referred to as "HDF".

\*Denotes a field with near-infrared imaging.

†Denotes a field with mid-infrared *Spitzer* IRAC imaging.

half of the observations described in Steidel et al. (2003, 2004) and half from subsequent programs by the same authors. These surveys employed photometric preselection in the  $U_n G \mathcal{R}$  passbands in a variety of fields (Reddy et al. 2008) to target galaxies in the redshift interval  $z \sim 2-3$ . Follow-up optical spectroscopy of a subset of these galaxies, paired with supplemental near and mid-infrared photometry, has yielded an extensive data set upon which multiple studies have been based (e.g., Shapley et al. 2003; Adelberger et al. 2005a; Shapley et al. 2005; Erb et al. 2006b; Reddy et al. 2008).

Here, we introduce a spectroscopic and photometric sample of  $z \sim 3$  LBGs. These data were photometrically preselected with the following standard LBG  $U_n G \mathcal{R}$  flux and color cuts:

$$\mathcal{R} \leq 25.5, \quad G - \mathcal{R} \leq 1.2, \quad U_n - G \geq G - \mathcal{R} + 1 \quad (1)$$

where the  $U_n$ ,  $G$ , and  $\mathcal{R}$  passbands sample  $\lambda_{\text{rest}} \sim 900$ , 1200, and 1700 Å at  $z \sim 3$ , respectively. Object detection, color cuts, and photometry are discussed in Steidel et al. (2003). Multi-object optical spectroscopy was obtained using the Low Resolution Imaging Spectrometer (LRIS; Oke et al. 1995) on the Keck I 10m telescope. The majority of the data (93%) were taken with the blue arm of LRIS (LRIS-B; McCarthy et al. 1998; Steidel et al. 2004), and the remainder of the data were obtained with LRIS prior to its blue arm upgrade in September 2000. The LRIS-B data were collected using 300, 400, and 600 line  $\text{mm}^{-1}$  grisms, which resulted in spectral resolutions of  $\lambda/\Delta\lambda = 1000$ , 1200, and 2000, respectively. The 400 (600) line  $\text{mm}^{-1}$  grism was used for 55% (39%) of the observations, and the remaining  $\sim 6\%$  of the LRIS-B spectra were obtained with the 300 line  $\text{mm}^{-1}$  grism. LRIS-B rest-frame wavelength coverage extended from  $\sim 900-1500$  Å and a typical integration time was  $3 \times 1800$  s. The data were reduced (flat-fielded, cosmic ray rejected, background subtracted, extracted, wavelength and flux

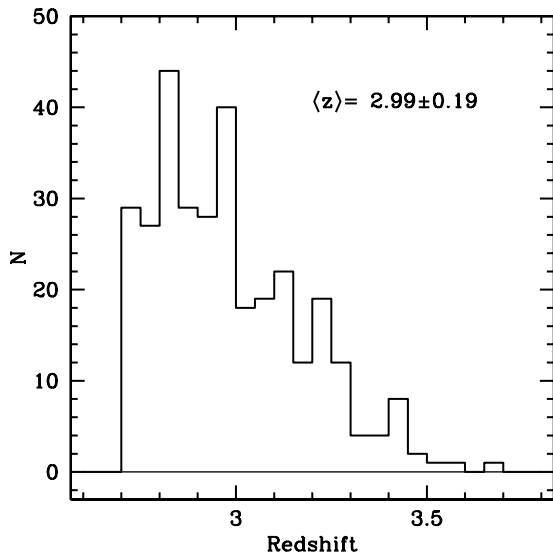


FIG. 1.— Redshift distribution of the sample, where  $\langle z \rangle = 2.99 \pm 0.19$ .

calibrated, and transformed to the vacuum wavelength frame) using IRAF scripts. Details of the data collection and reduction of both the preselection and spectroscopic samples are presented in Steidel et al. (2003).

Approximately 3% of the spectroscopically-confirmed  $z \sim 3$  LBGs were classified as either active galactic nuclei (AGN) or quasi-stellar objects (QSOs) on the basis of broad lines and high-ionization emission features, respectively (Reddy et al. 2008). These objects were excluded from the spectroscopic sample, as were galaxies at redshifts  $z \leq 2.7$ . The final sample, spanning 13 photometric preselection fields totaling 1700 arcmin<sup>2</sup>, includes 321 objects with an average redshift of  $\langle z \rangle = 2.99 \pm 0.19$  (Table 1, Figure 1). We note that this sample is distinct from previous studies of  $z \sim 3$  LBGs (e.g., Shapley et al. 2001, 2003) in that the majority of these objects have corresponding near- and mid-infrared photometry.

Near-infrared photometry in the  $J$  ( $\lambda_c = 1.25 \mu\text{m}$ ) and  $K_s$  ( $\lambda_c = 2.15 \mu\text{m}$ ) bands was obtained for a subset of the sample (8/13 fields) using the Wide Field Infrared Camera (Wilson et al. 2003) on the Palomar 5m telescope. 102/321 objects (32%) were detected in  $K_s$  imaging and an additional 69 objects fell on the  $K_s$  images and were not detected. We assigned  $K_s$  upper limits corresponding to  $3\sigma$  image depths ( $K_s \sim 22.2$  (Vega); Erb et al. 2006b) to these 69 galaxies.  $J$  band photometry was also obtained for 57/102 objects (56%) detected in the  $K_s$  sample. Details of the data collection and reduction of the near-infrared sample are presented in Shapley et al. (2005) and Erb et al. (2006b).

Mid-infrared imaging was obtained for 5/13 fields with IRAC on *Spitzer*. Observations at 3.6, 4.5, 5.8, and 8.0  $\mu\text{m}$  were obtained for the GOODS-N (Dickinson et al. 2003; Giavalisco et al. 2004; Reddy et al. 2006a), Q1700 (Shapley et al. 2005), and Q1549, Q1623, and Q2343 (Erb et al. in preparation) fields, where  $3\sigma$  IRAC detection limits ranged from 25.1–24.8 (AB). The mid-infrared data were reduced according to procedures described in Shapley et al. (2005). 112/321 objects (35%) have detections in at least one IRAC passband, and 34/321 objects (11%) have both  $K_s$  and IRAC detections.

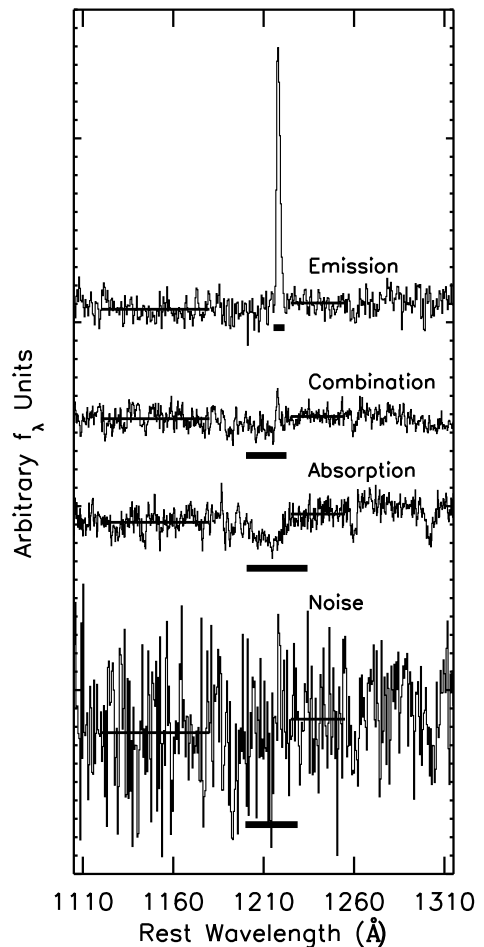


FIG. 2.— The Ly $\alpha$  feature varies widely in its morphology. Four spectra are plotted to show representative examples of objects classified in the “emission,” “combination,” “absorption,” and “noise” bins, respectively. In order to systematically calculate Ly $\alpha$  equivalent width, we adopted red- and blue-side continua (horizontal lines from 1120–1180 Å and from 1225–1255 Å, respectively) and inferred the extent of the Ly $\alpha$  feature (thick line below each spectrum) using the methodology described in §2.3. Note that in the case of the “absorption” spectrum shown here, the extent of the Ly $\alpha$  feature appears to extend rearwards of the adopted red-side continuum – this difference arises because the plotted spectrum is unsmoothed while a smoothed spectrum was employed to calculate the wavelength bounds of the Ly $\alpha$  feature.

## 2.2. Galaxy Systemic Redshifts

In order to prepare the spectra for subsequent measurement and analysis, we transformed each spectrum into the stellar systemic frame where the galaxy’s center of mass was at rest. To do so, we employed the procedure of Adelberger et al. (2003) to infer the galaxy’s systemic redshift from measurements of its redshifts of both Ly $\alpha$  in emission and interstellar lines in absorption. For the spectra that clearly exhibited a double-peaked Ly $\alpha$  emission feature (12/321 objects), we adopted the convention of setting the Ly $\alpha$  emission redshift equal to the average redshift of the two emission peaks. This technique of inferring a zero-velocity center-of-mass redshift, as opposed to measuring it directly, was necessary due to the fact that stellar lines arising from OB stars (assumed to be at rest with respect to the galaxy) are too weak to measure in individual spectra at  $z \sim 3$ . Furthermore, a

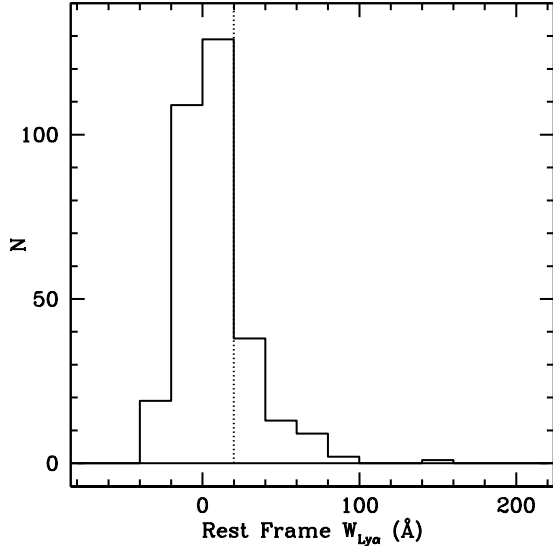


FIG. 3.— The distribution of Ly $\alpha$  rest-frame equivalent widths, where objects with  $W_{\text{Ly}\alpha} \geq 20$  Å (dashed line) were classified as LAEs. The median equivalent width of the sample is  $\sim 4$  Å, and an outlier at  $\sim 740$  Å (attributed to an uncertain continuum level) is not shown for visual clarity.

systemic redshift could not be measured from prominent LBG spectral signposts (e.g., Ly $\alpha$  or interstellar absorption lines) as these features trace outflowing gas which is offset from the galaxy’s center-of-mass frame by several hundred km s $^{-1}$  (Shapley et al. 2003).

### 2.3. Ly $\alpha$ Equivalent Width

HI Ly $\alpha$ , typically the strongest feature in LBG spectra, is characterized by its equivalent width,  $W_{\text{Ly}\alpha}$ , where we use a negative equivalent width to correspond to the feature in absorption. We present here a systematic method for estimating  $W_{\text{Ly}\alpha}$ , taking into account the various Ly $\alpha$  spectroscopic morphologies that were observed in the sample. In particular, this method employs a more robust technique than used previously to determine the wavelength extent over which the Ly $\alpha$  feature should be integrated to extract a line flux.

We first binned the 321 systemic-frame spectra into one of four categories based on the morphology of Ly $\alpha$ : “emission”, “absorption”, “combination”, and “noise”. The spectra in the “emission” bin were clearly dominated by a Ly $\alpha$  emission feature, and a small subset of this sample exhibited two peaks in emission. The spectra in the “absorption” bin were dominated by a trough around Ly $\alpha$ , typically extending for tens of angstroms bluewards of line center. The spectra deemed to be “combination” contained a Ly $\alpha$  emission feature superimposed on a larger Ly $\alpha$  absorption trough and the “noise” spectra were generally featureless around Ly $\alpha$ , save for a possible absorption signature whose secure identification was hindered by low signal-to-noise. Four example spectra, characterized as falling into each of these four bins, are shown in Figure 2.

Each spectrum, regardless of its category classification, was fit with two average continuum levels, one bluewards (1120–1180 Å;  $c_{\text{blue}}$ ) and one redwards (1225–1255 Å;  $c_{\text{red}}$ ) of Ly $\alpha$ ; these wavelength ranges were chosen to avoid the prominent Si III and Si II absorption features at 1206 and 1260 Å, respectively. We worked with both

the spectra and the adopted continua in  $f_{\lambda}$  units (erg s $^{-1}$  cm $^{-2}$  Å $^{-1}$ ). Below, we briefly describe the procedure for calculating  $W_{\text{Ly}\alpha}$  for each of the four morphological classification bins.

*Emission:* 189/321 objects (59%): The wavelength of the maximum flux value between 1213–1221 Å was calculated, as well as the wavelengths on either side of the maximum where the flux level intersected  $c_{\text{red}}$  and  $c_{\text{blue}}$ , respectively. These latter two wavelengths were adopted as the extremes of the emission feature. In a limited number of cases (12/188 objects), double-peaked spectra were individually examined to ensure that this methodology counted both peaks as contained within the Ly $\alpha$  feature. The IRAF routine SPLAT was next used to calculate the enclosed flux between the two wavelength bounds. The enclosed flux was then divided by the level of  $c_{\text{red}}$  to yield a measurement of  $W_{\text{Ly}\alpha}$  in Å. The level of  $c_{\text{blue}}$  was not used in the calculation of  $W_{\text{Ly}\alpha}$  due to its substantial diminution by the intergalactic medium (IGM).

*Absorption:* 50/321 objects (16%): The boundaries of the Ly $\alpha$  absorption feature were calculated in the same manner as those of the “emission” spectra described above, with the exception that the flux value between 1213 and 1221 Å was isolated as a minimum and the “absorption” spectra were initially smoothed with a boxcar function of width six pixels ( $\sim 2.5$  Å) in order to minimize the possibility of noise spikes affecting the derived wavelength boundaries of the Ly $\alpha$  feature. These smoothed spectra were only used to define the extent of the Ly $\alpha$  line; the original unsmoothed spectra were used for the flux integration in IRAF and the enclosed flux was divided by  $c_{\text{red}}$  to yield  $W_{\text{Ly}\alpha}$ .

*Combination:* 31/321 objects (10%): Objects in the “combination” bin were characterized by a Ly $\alpha$  emission feature superposed on a larger absorption trough. The boundaries of the Ly $\alpha$  feature were computed by beginning at the base of the Ly $\alpha$  emission peak and moving toward larger fluxes until the smoothed spectrum (see above) intersected  $c_{\text{red}}$  and  $c_{\text{blue}}$ , respectively (the same technique used for the “absorption” spectra). Flux integration and division by  $c_{\text{red}}$  were furthermore identical to those objects discussed above.

*Noise:* 51/321 objects (16%): For these spectra dominated by noise, we adopted set values for the endpoints of the Ly $\alpha$  feature based on the average boundary values of the absorption and combination spectra – 1199.9 and 1228.8 Å. (The boundaries of the “emission” spectra were not included in this calculation, as the spectral morphologies of the “emission” galaxies differed greatly from those of the “noise” galaxies). As above, the integrated flux was divided by the level of  $c_{\text{red}}$  to yield  $W_{\text{Ly}\alpha}$ .

Rest frame equivalent widths ranged from  $-40$  Å  $\lesssim W_{\text{Ly}\alpha} \lesssim 160$  Å, although one object (HDF-C41) had an equivalent width of  $\sim 740$  Å; we attributed this outlier to a continuum level in the spectrum comparable with zero and omitted this object from further analysis. The median equivalent width of the sample was  $\sim 4$  Å (Figure 3), consistent with values reported by Shapley et al. (2001, 2003) for  $z \sim 3$  LBGs.

### 2.4. Composite Spectra

A composite spectrum offers the distinct advantage of higher signal-to-noise over individual observations. We

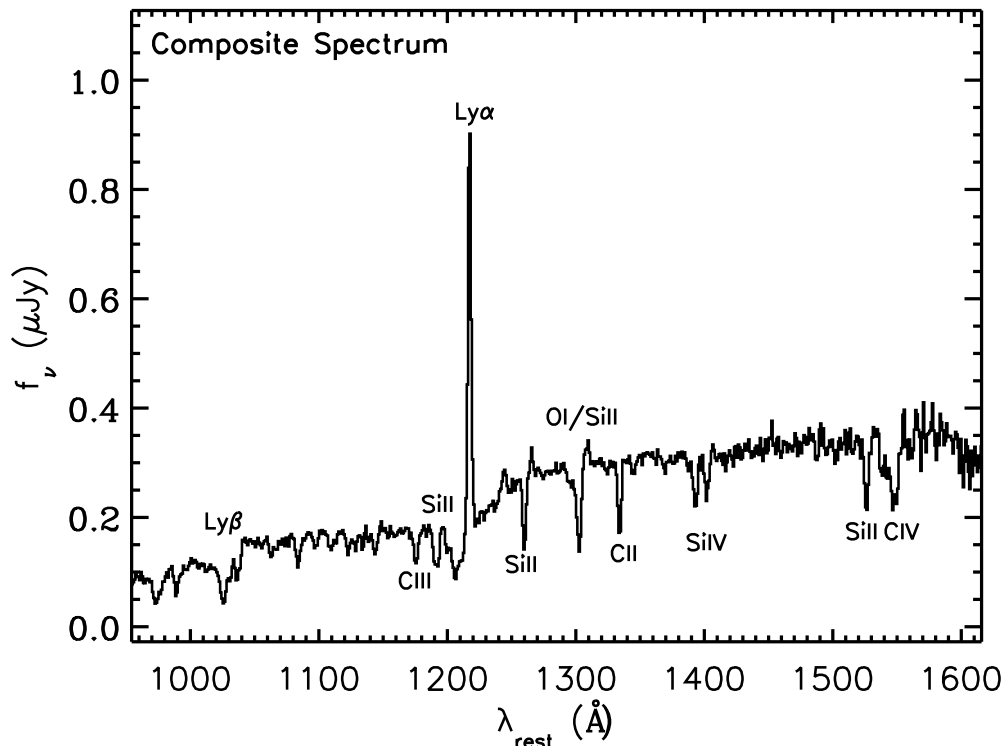


FIG. 4.— Composite rest-frame spectrum assembled from one-dimensional, flux-calibrated spectra (§2.4).  $\text{Ly}\alpha$  appears in strong emission and  $\text{Ly}\beta$  is prominent at 1026 Å. Photospheric features (e.g., CIII  $\lambda$ 1176) and both low- (e.g., SiII  $\lambda\lambda$ 1190,1193, SiII  $\lambda$ 1260, OI+SiII  $\lambda$ 1303, CII  $\lambda$ 1334, and SiII  $\lambda$ 1527) and high- (e.g., SiIV  $\lambda\lambda$ 1393,1402 and CIV  $\lambda$ 1549) ionization absorption lines are visible in this high signal-to-noise composite.

accordingly constructed several composite spectra from our sample, using, in each case, the same basic steps discussed below.

The one-dimensional, flux-calibrated, rest-frame input spectra of interest were stacked (mean-combined) using the IRAF `scombine` routine. Each input spectrum was scaled to a common mode over the wavelength range 1250–1380 Å and a small number of positive and negative outliers ( $< 10\%$  of the data) were rejected at each pixel position to prevent poor sky-subtraction or cosmic ray residuals from affecting the composite spectrum. The final composite spectrum was then rebinned to a dispersion of  $1 \text{ Å pixel}^{-1}$ . A composite spectrum<sup>7</sup> of the entire sample is shown in Figure 4, where several photospheric and low- and high-ionization interstellar features are visible in addition to  $\text{Ly}\alpha$ .

### 3. STELLAR POPULATION MODELING

As the majority of the spectroscopic sample had extensive accompanying photometric wavelength coverage, we conducted population synthesis modeling to derive the key properties of age, extinction, star formation rate, and

<sup>7</sup> This composite spectrum is meant to represent only the average of the objects in our sample, not the average of the entire  $z \sim 3$  LBG population. There are a variety of observational biases that affect that relative proportions of  $\text{Ly}\alpha$ -emitters and  $\text{Ly}\alpha$ -absorbers selected: large  $\text{Ly}\alpha$  emission lines contaminating the  $G$  band result in redder  $U_n - G$  colors, scattering objects into the color selection window (Equation 1), while  $\text{Ly}\alpha$  absorption limits the dynamic range in continuum magnitude over which objects are selected. We refer the reader to Steidel et al. (2003) for a detailed discussion of these biases.

stellar mass. We required at least one photometric measurement redwards of the Balmer break ( $\lambda_{\text{rest}} = 3646 \text{ Å}$ ) for robust population synthesis modeling. 248/320 objects satisfied this criterion of photometry in at least one near-infrared or IRAC passband, including 69 objects with  $K_s$  upper limits (and no IRAC data). We modeled galaxies using Bruzual & Charlot (2003) SEDs (assuming a Salpeter (1955) initial mass function (IMF) over the mass range  $0.1\text{--}125 M_{\odot}$ ) and the Calzetti (2000) extinction law derived from local starbursts, where dust extinction, parameterized by  $E(B-V)$ , was estimated from the latter. While the Calzetti et al. (2000) law appears valid on average for  $z \sim 3$  LBGs, we discuss in §4.2 some caveats associated with adopting this law. We furthermore assumed a constant star formation history and solar metallicity. Recent work has suggested that the Salpeter (1955) IMF has too steep a slope below  $1 M_{\odot}$  and consequently overpredicts the mass-to-light ratio and stellar mass by a factor  $\sim 2$  (Bell et al. 2003; Renzini 2006). We accordingly converted stellar masses and SFRs to the Chabrier (2003) IMF by dividing the model output values by 1.8. The modeling procedure is described in detail in Shapley et al. (2001); we briefly present a summary below.

Firstly, for the subset of the sample where  $\text{Ly}\alpha$  fell in the  $G$  bandpass ( $2.48 \lesssim z \lesssim 3.38$ ; 238/248 objects), we corrected the  $G$  band photometry to account for the discrepancy between the equivalent widths of the sample ( $-40 \text{ Å} \lesssim W_{\text{Ly}\alpha} \lesssim 160 \text{ Å}$ ) and those of the Bruzual & Charlot (2003) model SEDs ( $W_{\text{Ly}\alpha} \sim -10 \text{ Å}$ ). Accord-

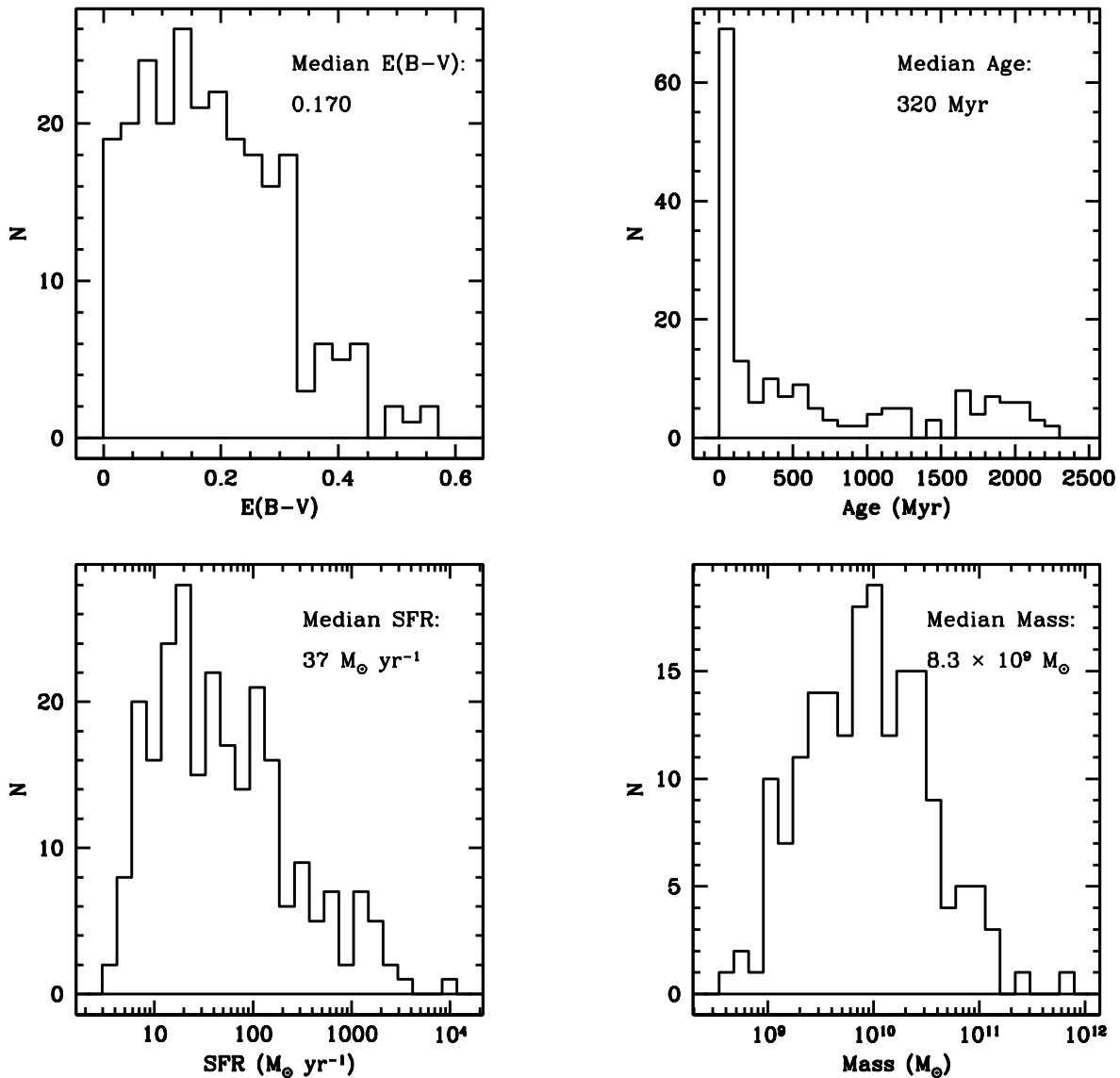


FIG. 5.— Histograms of best-fit stellar population parameters, with median values indicated.  $K_s$ -undetected galaxies were omitted when making the age and stellar mass distributions, as these parameters represent upper limits in the presence of a  $K_s$  non-detection. Dust attenuations span the range  $E(B-V) = 0.0$ – $0.6$ , where the median extinction level corresponds to  $A_{1600}$  ( $A_V$ )  $\sim 1.7$  (0.7) magnitudes. While LBGs are fit with a variety of ages, note the large number of objects in the youngest age bin,  $t_\star < 100$  Myr. The SFRs of LBGs fall between those of quiescent, Milky Way-type galaxies (SFR  $\sim 4 M_\odot \text{ yr}^{-1}$ ; e.g., Diehl et al. 2006) and vigorously star-forming submillimeter galaxies (SFR  $\sim 1000 M_\odot \text{ yr}^{-1}$ ; e.g., Chapman et al. 2005). Stellar masses range from  $\sim 10^9$  to  $10^{11} M_\odot$ , where the highest mass object,  $6 \times 10^{11} M_\odot$ , is extremely red ( $R - K_s = 4.48$ ).

ing to the formula in Papovich et al. (2001), we applied a correction in the cases where the incremental change in  $G$  magnitude,  $\Delta G$ , was larger than the uncertainty on the original photometric measurement. This procedure affected 51/238 objects (21%), for which  $\langle \Delta G \rangle_{\text{median}} = 0.15$  magnitudes. We did not correct for possible contamination in the  $K_s$  band from nebular line emission ([OIII]  $\lambda\lambda 5007, 4959$ , H $\beta$   $\lambda 4861$ ), although we tested that our reported correlations (§4) were still robust when all objects at  $z \geq 2.974$  (such that [OIII]  $\lambda 5007$ , the strongest of these nebular lines, is shifted into the  $K_s$  band) were excluded from the analysis.

Next, for each galaxy modeled, a grid of SEDs was at-

tenuated by dust and shifted to match the redshift of the galaxy. These redshifted SEDs were further attenuated by IGM absorption (Madau 1995) and were multiplied by the  $G, R, J, K_s$ , and four IRAC channel filter transmission curves to extract model colors. A model  $U_n - G$  color was not calculated, as many of the objects had only upper limits in  $U_n$  due to the significant flux diminution in that passband from both galactic and intergalactic HI absorption. These predicted colors were then compared with the observed colors by means of the  $\chi^2$  statistic and a best-fit  $E(B-V)$  and age ( $t_\star$ ) were extracted based on the lowest value of  $\chi^2$ . We also applied the constraint that  $t_\star$  had to be less than the age of the Universe at the

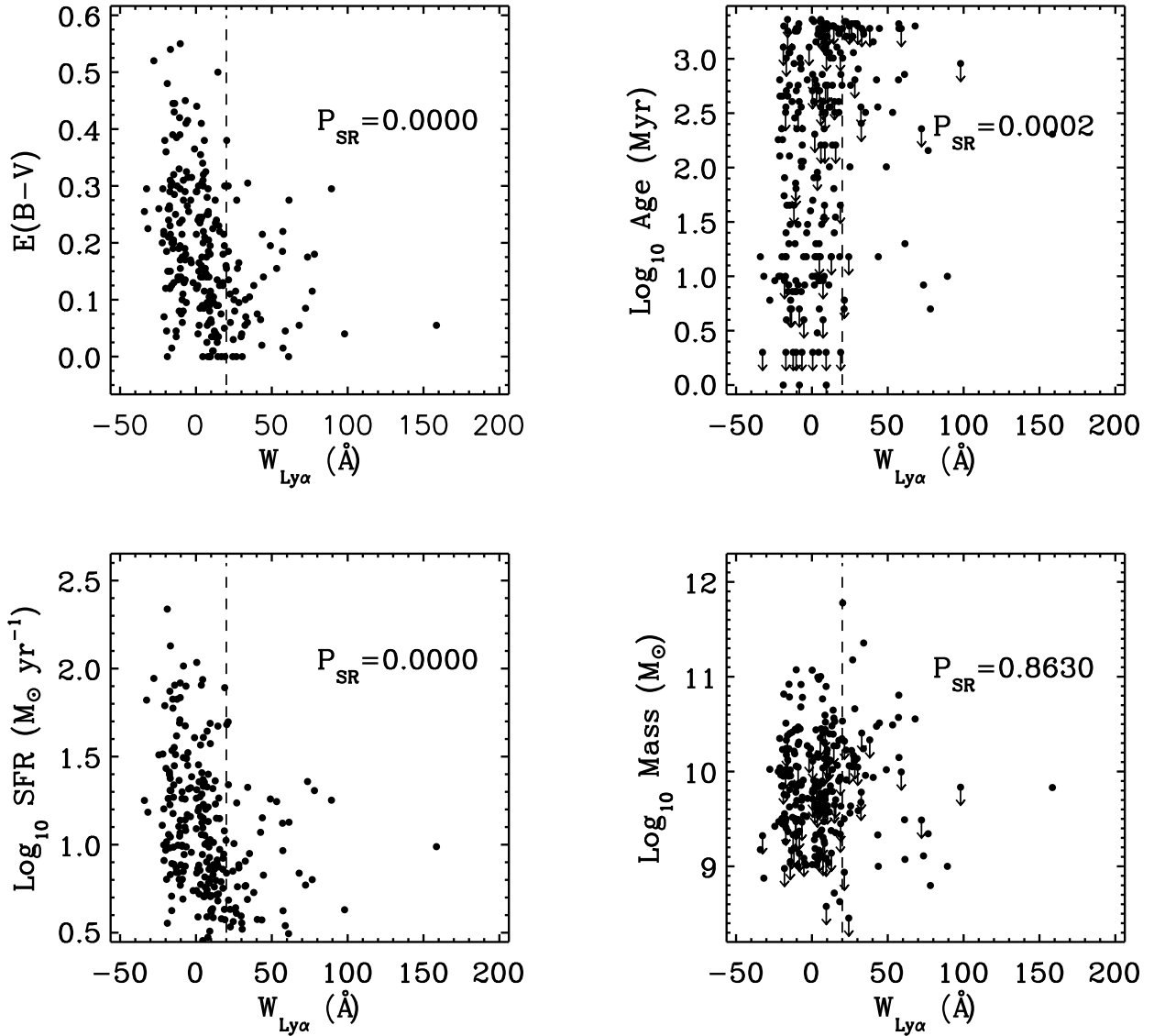


FIG. 6.— Plots indicating the correlation between  $W_{\text{Ly}\alpha}$  and each of the four best-fit stellar population parameters. Upper limits in age and mass are indicated by downward-facing arrows and the vertical dashed line in each panel delineates  $W_{\text{Ly}\alpha} = 20 \text{ \AA}$ , the adopted lower bound in  $\text{Ly}\alpha$  equivalent width for LAEs. The probability of a null hypothesis (i.e., no correlation) from the Spearman  $\rho$  test is shown in each plot. Note the significant correlation between equivalent width and E(B-V), age, and SFR, respectively, in the sense that galaxies with strong  $\text{Ly}\alpha$  emission also tend to be less dusty, older, and more quiescently forming stars.  $W_{\text{Ly}\alpha}$  and stellar mass are not significantly correlated, as evidenced by the high probability of the null hypothesis.

redshift of each object. A best-fit dust-corrected SFR was inferred from the normalization of a galaxy forming stars at a rate of  $1 M_{\odot} \text{ yr}^{-1}$ . Stellar mass,  $m_{\text{star}}$ , was defined as the integral of the SFR and the age of the galaxy. We did not correct stellar masses for interstellar medium (ISM) recycling, whereby a mass fraction of stellar material is returned to the ISM via winds and supernovae (Cole et al. 2000). Given that we are concerned with the relative stellar populations of objects modeled in an identical fashion, the constant mass factor introduced by assuming ISM recycling is unimportant.

Best-fit SFR, stellar mass, E(B-V), and age values were extracted for the 179 galaxies without photometric upper limits. The additional 69 galaxies undetected in  $K_s$  imaging were modeled by adopting  $3\sigma$  upper limits in  $\mathcal{R} - K_s$  color as photometric data points. We tested

that an upper limit in  $\mathcal{R} - K_s$  color was a robust proxy for an upper limit in both age and stellar mass by perturbing the  $\mathcal{R} - K_s$  colors in several increments, both redwards and bluewards, and re-modeling the perturbed SEDs (holding all other colors constant). The expected trend that a redder galaxy would be best fit with an older age and a larger stellar mass was borne out for the entire sample. We additionally found that E(B-V) and SFR were generally insensitive to perturbations in  $\mathcal{R} - K_s$  color. Therefore, given a galaxy with an upper limit in  $\mathcal{R} - K_s$  color, its model age and stellar mass were adopted as upper limits and its model E(B-V) and SFR were assumed to be best-fit values.

Considering the entire sample of 248 objects, we found median best-fit SFR, stellar mass, E(B-V), and age values of  $37 M_{\odot} \text{ yr}^{-1}$ ,  $7.2 \times 10^9 M_{\odot}$ , 0.170, and 320 Myr, re-



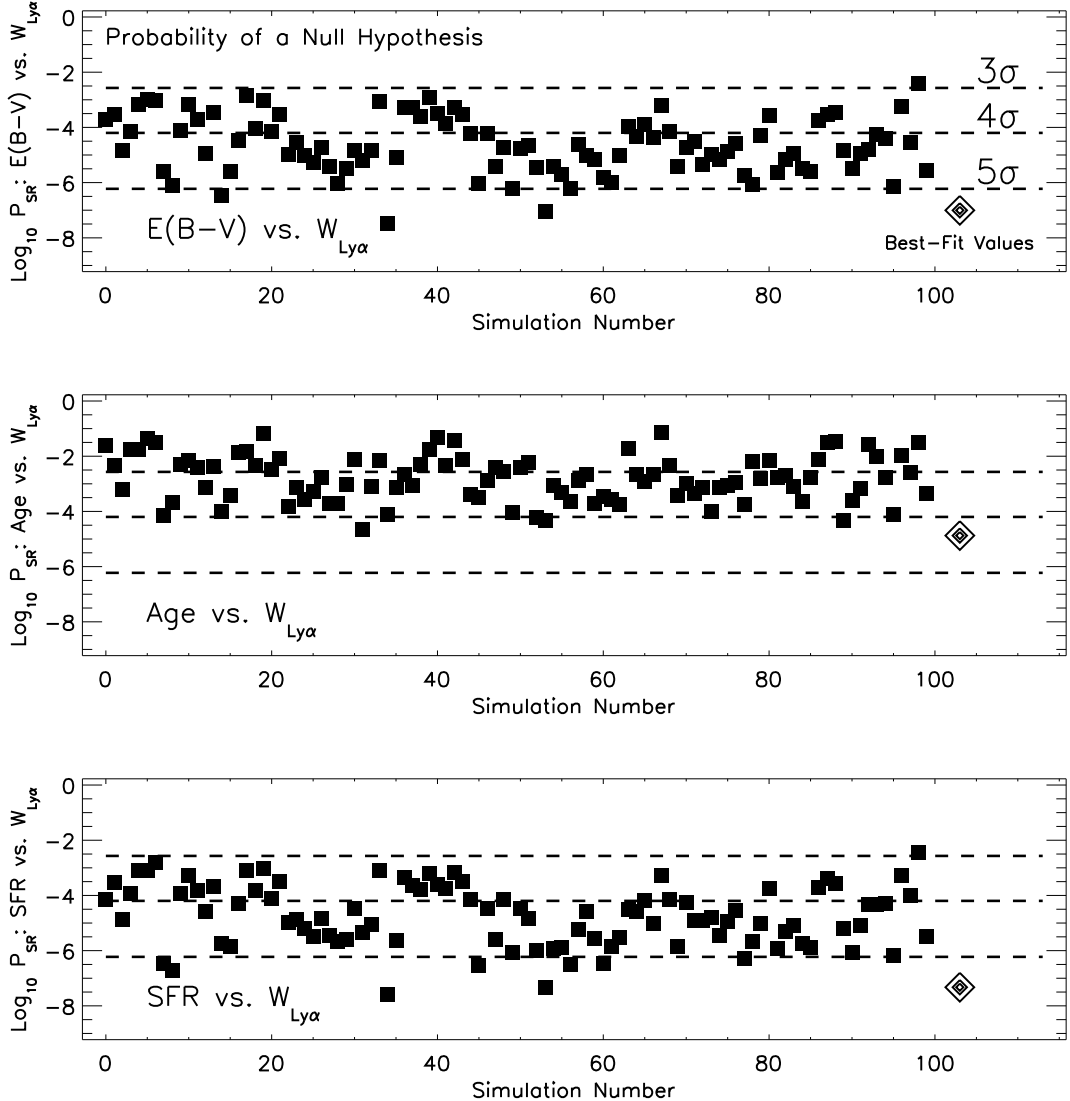


FIG. 7.— Probability of a null hypothesis (i.e., no correlation) between  $W_{\text{Ly}\alpha}$  and E(B-V), age, and SFR, respectively. The probabilities from 100 simulated data sets are shown, where the simulated data sets were made by extracting one line from each of the 34 LAE and 145 non-LAE confidence intervals (§3). The horizontal dashed lines correspond to 3, 4, and 5 $\sigma$  levels and the probabilities from the best-fit values are shown as the diamond data point on the far right of each plot. These data show that  $W_{\text{Ly}\alpha}$  is correlated with E(B-V), age, and SFR, respectively, even when accounting for the uncertainties in the best-fit stellar population parameters. The average probability of a null hypothesis between  $W_{\text{Ly}\alpha}$  and stellar mass (not shown) would have a value of approximately  $-0.1$  on these plots ( $\sim 1\sigma$ ).

spectively. When objects with  $K_s$  upper limits (and corresponding upper limits in stellar age and mass) were removed from the analysis, the medians were  $51 M_{\odot} \text{ yr}^{-1}$ ,  $8.3 \times 10^9 M_{\odot}$ , 0.180, and 320 Myr, respectively. A dust attenuation described by  $E(B-V) = 0.170$  corresponds to  $A_V \sim 0.7$  magnitudes, using the Calzetti et al. (2000) starburst attenuation law with  $R'_V = 4.05$ . Histograms of the best-fit values are shown in Figure 5.

For each galaxy, confidence intervals of the best-fit stellar parameters were estimated with Monte Carlo simulations. First, each object’s photometry was perturbed by an amount drawn from a Gaussian distribution described by the photometric error. Then, the galaxy was remodeled with these new “observed” colors, and this process was repeated 1000 times. These simulations resulted in estimates of the distributions of best-fit stellar parameters allowed by the uncertainties in the photometry. In some instances, these confidence intervals were

not centered on the best-fit stellar population parameters derived from fitting the photometry. In all cases, we proceeded to adopt the best-fit values as representative of each galaxy’s properties, and we furthermore assumed that the error on each parameter was described by the standard deviation of that parameter’s confidence interval. We used the quantity  $\sigma_x/\langle x \rangle$  to express the ratio of the standard deviation of each parameter’s confidence interval,  $\sigma_x$ , to the mean of that parameter’s confidence interval,  $\langle x \rangle$ . On average, using 3 $\sigma$  rejection to suppress the effect of outliers, we found that the median values of  $\sigma_x/\langle x \rangle$  for each of the four best-fit stellar population parameters (E(B-V), age, SFR, and stellar mass) were  $\sim 0.4$ , 1.0, 0.8, and 0.6, respectively.

#### 4. STELLAR POPULATIONS & $\text{Ly}\alpha$ LINE STRENGTH

With  $\text{Ly}\alpha$  equivalent widths and best-fit stellar population parameters in hand, we now turn to examining

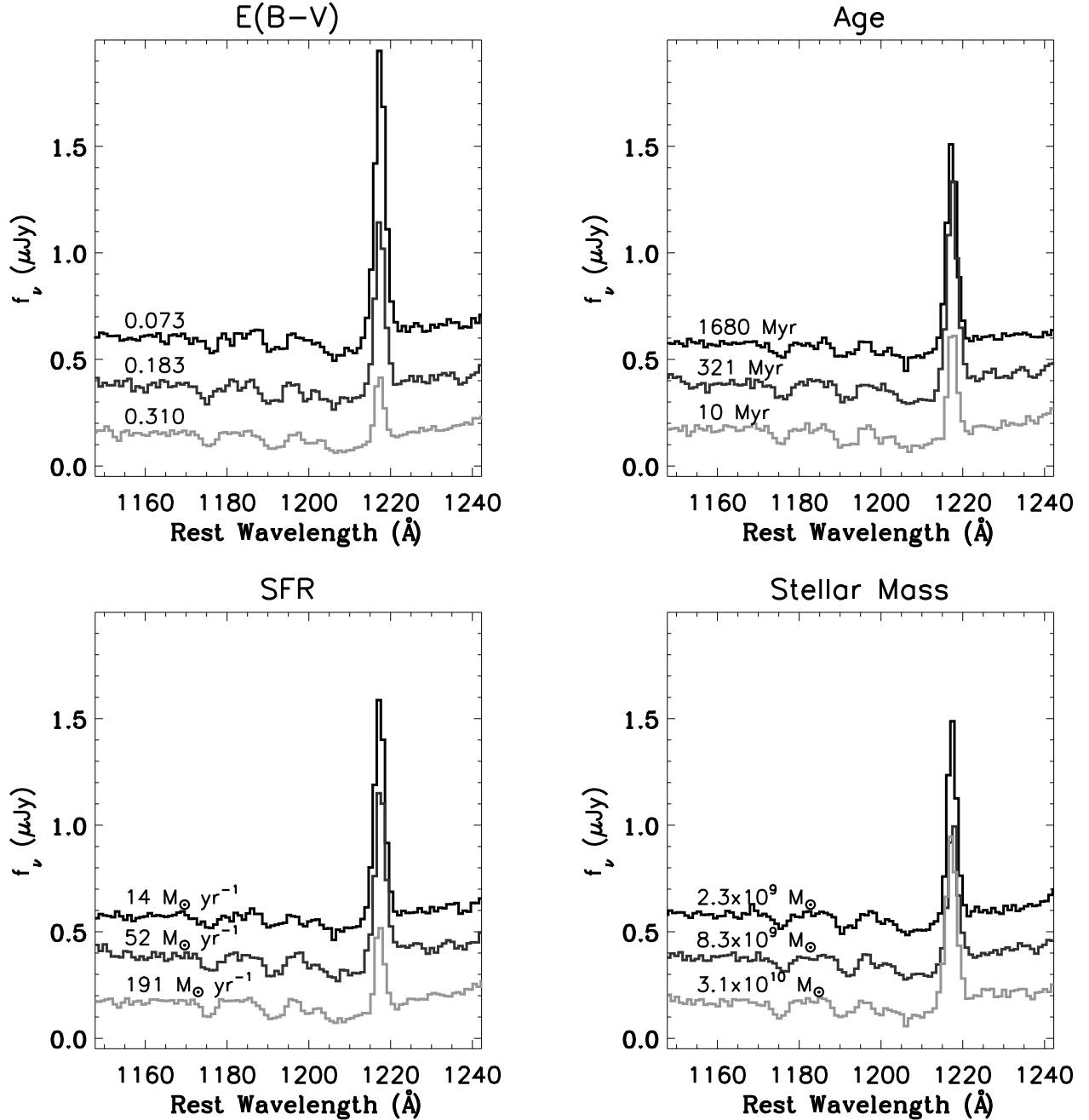


FIG. 8.— Composite spectra assembled from objects ordered by  $E(B-V)$ , age, SFR, and stellar mass, respectively, where objects with  $K_s$  upper limits were omitted. The medium and dark gray spectra are offset by  $+0.2$  and  $+0.4 \mu\text{Jy}$ , respectively, from the light gray spectrum and the median value in each tertile is printed next to its composite. Notice how strong  $\text{Ly}\alpha$  emission is associated with older, less dusty, and more quiescent galaxies. There does not appear to be a significant correlation between  $\text{Ly}\alpha$  emission strength and best-fit stellar mass.

the relationship between  $\text{Ly}\alpha$  emission and stellar populations in LBGs. The aim of this analysis is to investigate the physical nature of  $z \sim 3$  LBGs by studying how objects with and without strong  $\text{Ly}\alpha$  emission differ in the fundamental parameters of age, stellar mass, extinction, and star formation rate. Our full complement of data are used in this analysis, including rest-frame UV spectroscopy, broadband photometry, and best-fit stellar population parameters and SEDs. We also make comparisons between our LBG data and narrowband-selected LAEs from Nilsson et al. (2007) and Gawiser et al. (2007), although we caution that the relationship between LBGs and narrowband-selected LAEs is a field

of extragalactic research unto itself; we refer the reader to §5.1 for a summary of the salient points of this topic.

#### 4.1. Statistical Tests

We employed several statistical methods central to our investigation, including survival analysis techniques that were capable of analyzing data with limits (“censored data”). It was important to include limits in the statistical analysis as a non-negligible fraction of the sample (28%) was undetected in  $K_s$  imaging. We used ASURV (“Astronomy SURVival Analysis”) Rev 1.2 (Isobe & Feigelson 1990; Lavalley et al. 1992), which implements the methods presented in Feigelson & Nelson (1985)

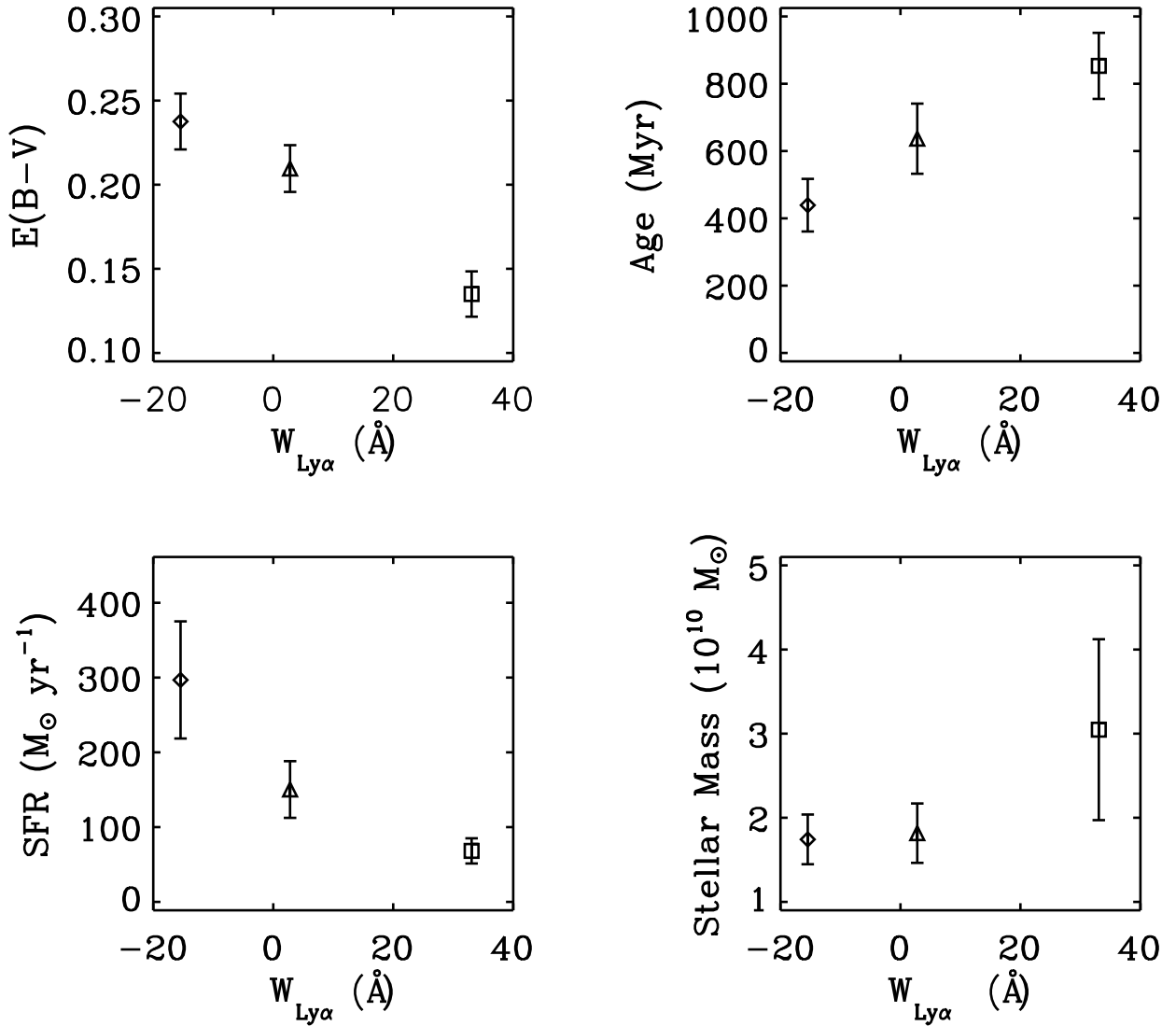


FIG. 9.— Best-fit stellar population parameters versus rest-frame  $\text{Ly}\alpha$  equivalent width. Omitting galaxies with  $K_s$  upper limits, the remaining 179 objects with stellar population modeling were ordered by equivalent width and divided into three groups. The average stellar population parameters of each group were extracted, along with the error on the mean ( $\sigma/\sqrt{n}$ , where  $n$  was the number of objects in each group). With increasing  $\text{Ly}\alpha$  strength, galaxies are, on average, older, less dusty, and more quiescent. A weak trend of increasing stellar mass with increasing  $\text{Ly}\alpha$  strength is observed, although this is likely not a significant correlation.

and Isobe et al. (1986). The bivariate correlation tests Kendall  $\tau$  and Spearman  $\rho$  were utilized, where, for each test, the degree of correlation is expressed in two variables:  $\tau_K$  ( $r_{\text{SR}}$ ) and  $P_K$  ( $P_{\text{SR}}$ ). The first variable represents the test statistic and the second variable represents the probability of a null hypothesis (i.e., the probability that the data are uncorrelated). We also used routines from Numerical Recipes (Press et al. 1992), specifically the Kolmogorov-Smirnov (K-S) test between two data sets (`kstwo`), the Spearman’s rank correlation (`spear`), and the Kendall’s  $\tau$  correlation (`kend11`). The K-S test produces two outputs:  $D$  and  $P$ , where the former is the test statistic and the latter is the probability that the two samples are drawn from the same underlying population. `spear` and `kend11` are duplicates of the Spearman  $\rho$  and Kendall  $\tau$  tests available in ASURV; we employed the ASURV routines when it was necessary to include data with limits.

#### 4.2. Equivalent Width Versus Stellar Parameters

Firstly, we investigated the correlation between  $\text{Ly}\alpha$  equivalent width and extinction, age, star formation rate, and stellar mass, respectively, using the Spearman  $\rho$  and Kendall  $\tau$  bivariate correlation tests. For this analysis, we used the entire sample with population modeling, including galaxies with upper limits in the  $K_s$  passband (248 objects). We note that while the correlations shown in Figure 6 are not without scatter, we have employed a variety of quantitative statistical analyses that have yielded a consistent picture of how stellar populations are correlated with  $\text{Ly}\alpha$  emission in  $z \sim 3$  LBGs. Below, we introduce these results.

$E(B-V)$ , age, and SFR all exhibited very strong correlations with  $W_{\text{Ly}\alpha}$  ( $P_{\text{SR}} \leq 0.0002$  in each case)<sup>8</sup>, whereas stellar mass was uncorrelated ( $P_{\text{SR}} = 0.8630$ ). These re-

<sup>8</sup> We note, however, that SFR and  $E(B-V)$  are not independent;

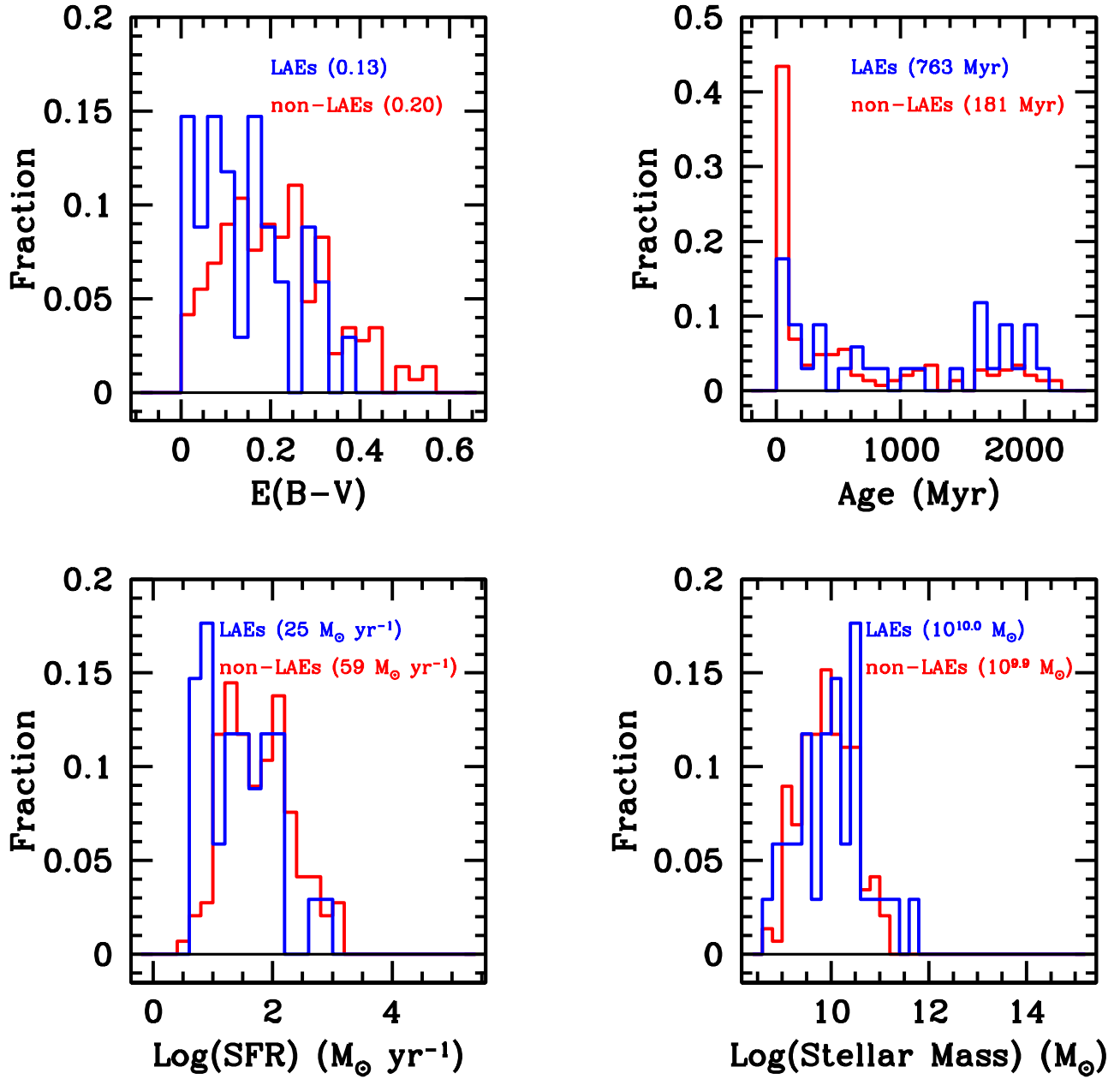


FIG. 10.— Histograms of best-fit dust attenuations, ages, star formation rates, and stellar masses for the 34 LAEs (blue line) and 145 non-LAEs (red line), non-inclusive of objects with  $K_s$  upper limits. The ordinate is the fractional percentage of the sample and the median value of each sample is indicated. The LAE sample is characterized by lower dust attenuation levels than the non-LAE sample; all objects with  $E(B-V) \geq 0.40$  are non-LAEs. The median age (763 Myr) of LAEs is significantly older than that of the non-LAEs (181 Myr). Furthermore, the LAEs lack the conspicuous overdensity of objects in the youngest ( $t_* < 100$  Myr) age bin that characterizes the non-LAE distribution. While the fraction of LAEs and non-LAEs with star formation rates between  $\sim 80$ – $120 M_\odot \text{ yr}^{-1}$  is roughly the same, LAEs show a larger fraction of objects with small SFRs and non-LAEs exhibit a tail of high star formation rate objects. LAEs are marginally more massive than non-LAEs, on average, although the distributions are similar.

sults did not change when the 69 galaxies with  $K_s$  upper limits (and corresponding upper limits in mass and age) were excluded from the analysis (Table 2). In order to test the robustness of these results while taking into account the uncertainty on the best-fit parameters, we used the bootstrapping method. We created 100 bootstrap samples by randomly extracting one line from each

the probability that these two parameters are uncorrelated is  $P_{\text{SR}} = 0.0000$ .

object’s 1000-entry confidence interval of stellar parameters (generated by perturbing the initial photometry according to its errors and then re-modeling the galaxy; §3) and then re-ran the Spearman  $\rho$  test on each of these 100 artificial samples. A null hypothesis was consistently ruled out at between the 3 and  $5\sigma$  levels for the SFR and  $E(B-V)$  bootstrap samples and at the  $3\sigma$  level for the age sample (Figure 7). In the case of the stellar mass sample, where the null hypothesis was ruled out at only the

TABLE 2  
CORRELATION COEFFICIENTS

Parameter	Parameter	Kendall $\tau$ $\tau_K^a$ ( $P_K$ ) <sup>b</sup>	Spearman $\rho$ $r_{SR}^a$ ( $P_{SR}$ ) <sup>b</sup>
Entire Sample (248 objects)			
$W_{Ly\alpha}$	E(B–V)	6.585 (0.0000)	–0.413 (0.0000)
.....	Age	3.655 (0.0003)	0.238 (0.0002)
.....	SFR	6.515 (0.0000)	–0.410 (0.0000)
.....	Stellar Mass	0.358 (0.7205)	0.011 (0.8630)
Omitting $K_s$ non-detections (179 objects)			
$W_{Ly\alpha}$	E(B–V)	5.163 (0.0000)	–0.385 (0.0000)
.....	Age	4.122 (0.0000)	0.319 (0.0000)
.....	SFR	5.299 (0.0000)	–0.394 (0.0000)
.....	Stellar Mass	0.917 (0.3592)	0.068 (0.3641)

<sup>a</sup>Test statistic.

<sup>b</sup>Probability of a null hypothesis (i.e., the probability that a correlation is not present).

1 $\sigma$  level, the data do not support a correlation between  $W_{Ly\alpha}$  and stellar mass. These bootstrap samples show that even when accounting for the uncertainty in best-fit parameters, a strong correlation exists between equivalent width and age, E(B–V), and SFR, respectively, such that objects with strong Ly $\alpha$  emission tend to be older, less dusty, and lower in star formation rate (more quiescent) than objects with weak or no Ly $\alpha$  emission.

As an independent test of the above results, we next used the rest-frame UV spectra to investigate how the morphology of the Ly $\alpha$  feature was, qualitatively, correlated with best-fit stellar population parameters. For this analysis, we limited our study to objects satisfying two criteria: 1) population synthesis modeling had been completed and 2)  $K_s$  photometry consisted of detections, not upper limits<sup>9</sup>. Together, these criteria isolated 179 objects. For each stellar population parameter, we divided the objects into three groups (“tertiles”) based on their best-fit value. A composite rest-frame UV spectrum was then constructed from each tertile according to the methodology presented in §2.4, for a total of 12 composite spectra (3 tertiles  $\times$  4 parameters; Figure 8). A strong correlation of equivalent width with age, E(B–V), and SFR was observed, such that stronger Ly $\alpha$  emission was more prevalent in older, less dusty, and more quiescent galaxies. At the same time, the strength of low-ionization interstellar absorption lines decreased with increasing Ly $\alpha$  emission strength (Shapley et al. 2003). We note that these trends were still present when the spectra were median-combined to make to the composites (as opposed to mean-combined).

Next, we reversed the independent and dependent variables from the previous investigation and, this time, divided the sample into tertiles according to Ly $\alpha$  equivalent width. The mean equivalent widths of each tertile were –15.5, 2.8, and 33.1 Å, respectively. We then calculated the average stellar parameters of each tertile, in addition to the error on the mean (Figure 9). Consistent with the

results of the bivariate correlation tests and the composite spectra divided by stellar population parameters discussed above, we found that as the average equivalent width varied from –15.5 Å to 33.1 Å,  $\langle t_\star \rangle$  increased from 440 Myr to 850 Myr,  $\langle E(B-V) \rangle$  decreased from 0.24 to 0.14, and  $\langle SFR \rangle$  decreased from 300  $M_\odot$  yr<sup>–1</sup> to 70  $M_\odot$  yr<sup>–1</sup>. A weak positive correlation between best-fit stellar mass and equivalent width was observed, although, given the errors on the average masses, we chose to adopt the stance that stellar mass was generally insensitive to changes in equivalent width.

From the three aforementioned investigations, a consistent picture has emerged: strong Ly $\alpha$  emission is associated with galaxies that are older, less dusty, and more quiescent than their counterparts with weaker Ly $\alpha$  emission or the line in absorption. We note that the trend of increasing Ly $\alpha$  strength with decreasing E(B–V) is a well-known result (e.g., Shapley et al. 2003; Reddy et al. 2006b; Pentericci et al. 2007). Deharveng et al. (2008), however, found no apparent correlation between Ly $\alpha$  equivalent width and UV color in a sample of 96 LAEs at  $z \sim 0.3$ , although we caution that the transformation from UV color to E(B–V) is sensitive to the geometry of the emitting stars and absorbing dust and may therefore not be constant for a heterogeneous population such as LAEs (e.g., Witt & Gordon 2000; Granato et al. 2000). The relationship between age and  $W_{Ly\alpha}$  observed in our data – older objects exhibiting stronger Ly $\alpha$  emission than younger objects – is in agreement with the results of Shapley et al. (2003). The inverse correlation between dust-corrected SFR and  $W_{Ly\alpha}$  that we observe has been noted by several authors as well (e.g., Ando et al. 2004; Reddy et al. 2006b; Tapken et al. 2007), although Nilsson et al. (2007) report a  $\sim 2\sigma$  direct correlation between SFR and  $W_{Ly\alpha}$  in a sample of 24 LAEs at  $z \sim 3.15$ . In contrast with the results presented here, however, Erb et al. (2006a) reported a correlation between stellar mass and Ly $\alpha$  strength in a sample of 87 star-forming galaxies at  $z \sim 2$ . These authors found that composite spectra constructed from the 30 least massive galaxies ( $\langle M \rangle = 5 \times 10^9 M_\odot$ ) and the 28 most massive galaxies ( $\langle M \rangle = 7 \times 10^{10} M_\odot$ ) in their sample differed widely in nebular line strength, with the former sample exhibiting a pronounced Ly $\alpha$  emission feature and the latter sample showing a smaller Ly $\alpha$  feature superimposed on a larger absorption trough. Erb et al. (2006a) attributed these results to the lower velocity dispersion of the interstellar medium in the less massive galaxies, where, following the arguments of Mas-Hesse et al. (2003), velocity dispersion and Ly $\alpha$  escape fraction are anti-correlated. We therefore conclude here that the observed correlations we find between  $W_{Ly\alpha}$  and E(B–V), SFR, and age are supported by the work of others, whereas the lack of correlation between stellar mass and  $W_{Ly\alpha}$  may either be a tenable result (and evidence of LBG evolution during the 1.1 Gyr intervening  $z = 2$  and  $z = 3$ ) or otherwise an indication that further studies of the relationship between  $W_{Ly\alpha}$  and stellar mass at  $z \sim 3$  are necessary.

The correlations discussed above were derived assuming the Calzetti et al. (2000) dust attenuation law. While this relation has routinely been applied to samples of high-redshift galaxies (e.g., Erb et al. 2006b; Gawiser et al. 2006; Gronwall et al. 2007), recent work by Reddy et al. (2006b), based on *Spitzer* MIPS observations, has

<sup>9</sup> Objects with  $K_s$  upper limits were excluded due to their corresponding upper limits in best-fit ages and masses; such limits led to uncertainty as to the age and mass bin in which these objects should be grouped.

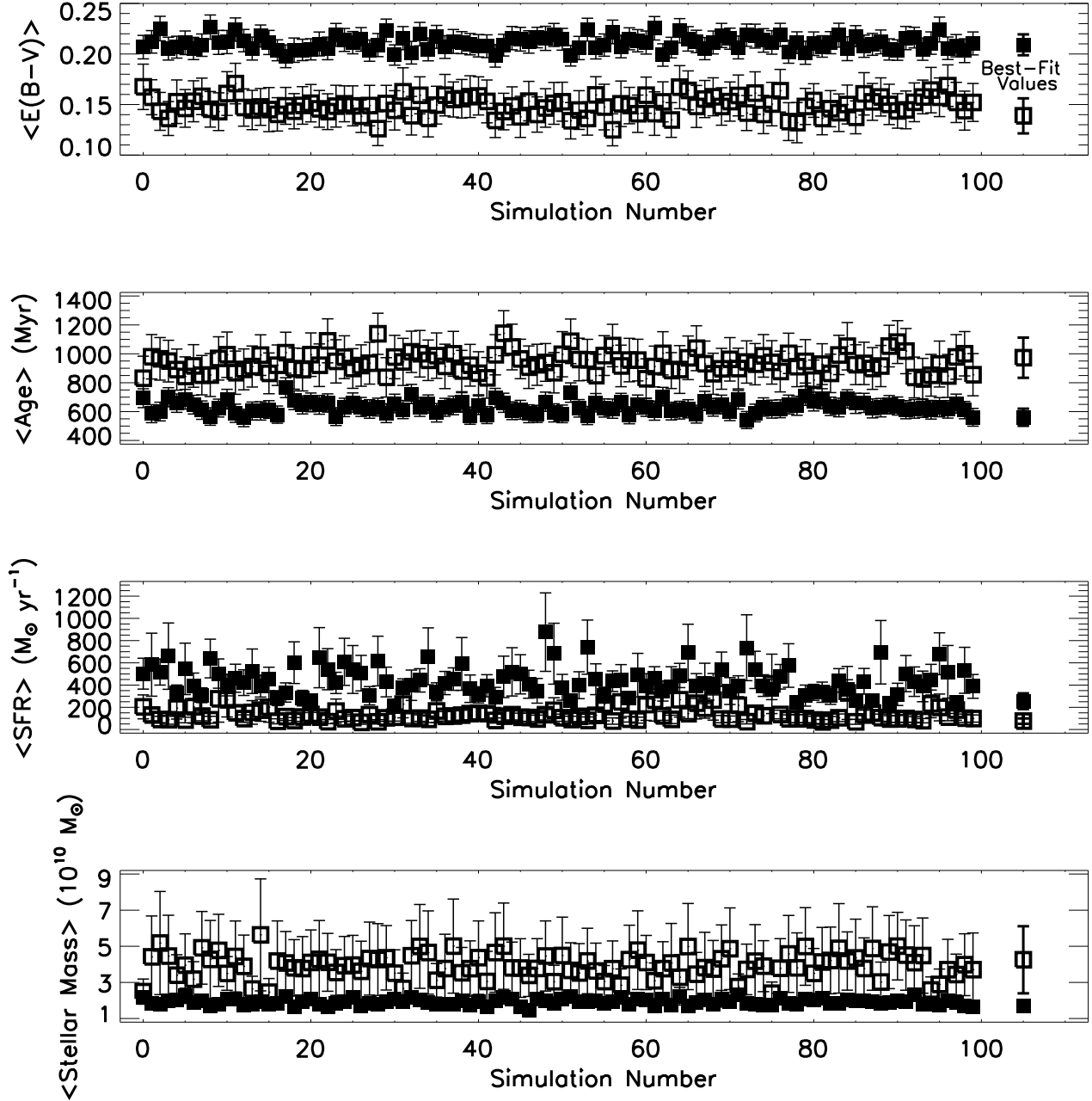


FIG. 11.— Average values of LAE and non-LAE best-fit stellar population parameters, extracted from 100 simulated data sets consisting of one line from each of the 34 LAE and 145 non-LAE confidence intervals (§3). Points corresponding to LAEs are shown as outlines and non-LAE data points are shown in solid black. The points to the far right are those corresponding to the actual best-fit values. These results show that the discrepancies between LAE and non-LAE stellar populations are significant, even when taking into account the uncertainties in the best-fit values. LAEs are, on average, less attenuated, older, and more quiescent than non-LAEs.

suggested that dust extinction in young ( $t_* \leq 100$  Myr), UV-selected galaxies at  $z \sim 2$  is often overestimated by modeling a given rest-frame UV color with the Calzetti et al. (2000) attenuation law. At  $z \sim 3$ , there have been no corresponding statistical studies, but Siana et al. (2008, 2009) have presented preliminary evidence for a similar trend based on two strongly-lensed objects. On the other hand, for a single unlensed LBG at  $z \sim 2.8$ , Chapman & Casey (2009) find good agreement between the dust extinction inferred from the Calzetti et al. (2000) law and that estimated from the ratio of SCUBA 850  $\mu\text{m}$  and rest-frame UV fluxes. Based on their find-

ings, Reddy et al. (2006b) and Siana et al. (2008) accordingly proposed that a steeper, SMC-like extinction relation (e.g., Prévot et al. 1984) may be more appropriate for young objects.

With these results in mind, we assessed the uncertainties inherent in the choice of attenuation law. Limiting our analysis to the 179 objects without  $K_s$  upper limits, we re-modeled the 70 galaxies with  $t_* \leq 100$  Myr with a SMC-like extinction law (and retained the original fits assuming the Calzetti et al. (2000) law for the remaining 109 objects). In this mixed sample with some objects modeled with a SMC-like law and others mod-

eled with the Calzetti et al. (2000) relation, we found no significant correlations between  $W_{\text{Ly}\alpha}$  and stellar populations. We also investigated the effect of re-modeling all 179 galaxies, regardless of age, with a SMC-like attenuation law. In this case, we observed correlations between  $W_{\text{Ly}\alpha}$  and  $E(B-V)$  and between  $W_{\text{Ly}\alpha}$  and SFR. Given the uncertainties in adopting the SMC law for part or all of our sample, another approach consists of restricting our analysis to objects for which the validity of the Calzetti et al. (2000) law has not been questioned. When we omitted objects younger than  $t_* = 100$  Myr from our original analysis assuming the Calzetti et al. (2000) dust attenuation law, the trends between  $W_{\text{Ly}\alpha}$  and  $E(B-V)$ , age, and SFR, respectively, were still present (but only at a  $2\sigma$  level of significance).

Given the lack of systematic studies of the dust attenuation law in  $z \sim 3$  objects, and the uncertainty regarding the age at which a galaxy may transition from being fit with a SMC-like law to the Calzetti et al. (2000) law, we choose to present all analysis on results derived from assuming the Calzetti et al. (2000) attenuation law. We acknowledge that the choice of an extinction law is a systematic uncertainty in our analysis, yet the persistence of trends between  $\text{Ly}\alpha$  and stellar populations in the sample limited to objects with  $t_* \geq 100$  Myr supports the analysis with the Calzetti law applied to the full sample.

In the next section, we divide the LBGs into two groups according to  $\text{Ly}\alpha$  strength and compare the stellar populations of these subgroups in order to more generally comment on the differences between objects with and without strong  $\text{Ly}\alpha$  emission.

#### 4.3. The Distinct Properties of Strong $\text{Ly}\alpha$ Emitters in the LBG Sample

From the perspective of examining  $\text{Ly}\alpha$  emission, the simplest division of our data is according to  $\text{Ly}\alpha$  equivalent width. We turn here to comparing the properties of objects with strong ( $W_{\text{Ly}\alpha} \geq 20$  Å)  $\text{Ly}\alpha$  emission and with weak  $\text{Ly}\alpha$  emission, or the line in absorption ( $W_{\text{Ly}\alpha} < 20$  Å). Given our large sample size, these two groups each have sufficient membership to ensure robust statistics even when we restrict our analysis to only those objects with both stellar population modeling and no  $K_s$  upper limits (34 and 145 objects, respectively). We call these two groups LAEs and non-LAEs, respectively, where we differentiate these objects from LAEs isolated with narrowband filters by explicitly referring to the latter as narrowband-selected objects. The motivation for choosing 20 Å as the delineating equivalent width stems from the adoption of this value as a typical limit in narrowband LAE studies (e.g., Gawiser et al. 2007; Nilsson et al. 2009b; Pentericci et al. 2009). In order to investigate how stellar populations vary between LAEs and non-LAEs, we examined the age,  $E(B-V)$ , stellar mass, and SFR distributions of both samples (Figure 10). We discuss below the striking differences between the properties of UV continuum-bright LAEs and non-LAEs.

There is a remarkable dissimilarity between the age histograms of LAEs and non-LAEs: LAEs are generally fit with older best-fit ages than non-LAEs: LAEs have a median age more than four times that of the non-LAEs (763 Myr versus 181 Myr). LAEs furthermore lack the conspicuous overdensity of young objects ( $t_* < 100$  Myr) that characterizes the non-LAE sample. The disparity in

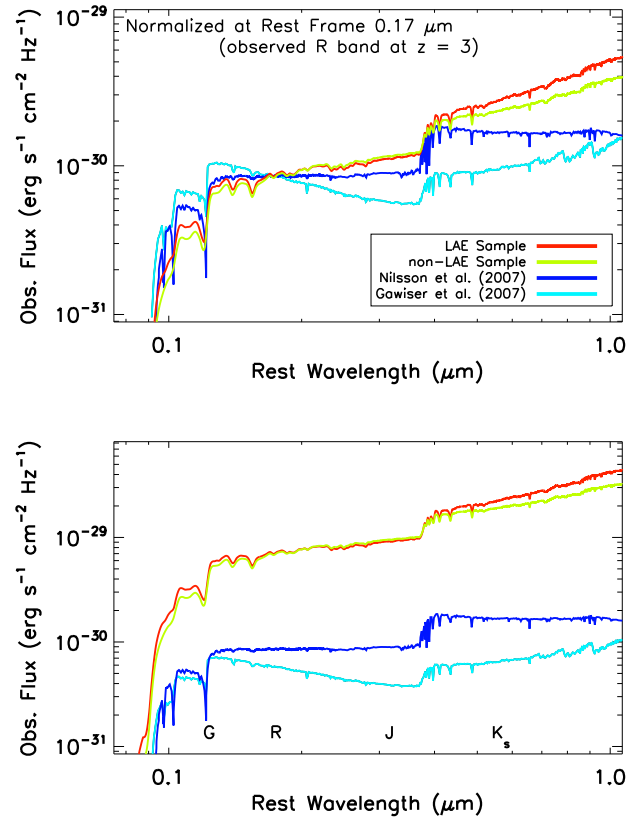


FIG. 12.— *Top panel:* Composite rest-frame UV to near-infrared SEDs of the LAE and non-LAE samples, assembled from best-fit SEDs from population synthesis modeling (omitting galaxies with  $K_s$  upper limits). Data from  $z \sim 3.1$  narrowband-selected LAEs (Nilsson et al. 2007; Gawiser et al. 2007) are overplotted and all spectra have been normalized to the Nilsson et al. (2007) flux value at  $0.17 \mu\text{m}$  (observed  $R$  band at  $z \sim 3$ ). Note that the LBG-selected objects have significantly redder  $G-R$  and  $R-K_s$  colors than the narrowband-selected LAEs, consistent with the older ages and higher dust attenuations derived for LBGs in the literature. *Bottom panel:* Un-normalized spectra; note the significant flux discrepancy ( $\sim 2.3$  magnitudes) between the color-selected LBGs and the narrowband-selected LAEs.

ages between LAEs and non-LAEs is reflected in the K-S test probability of  $\sim 2\%$  that the two age samples are drawn from the same underlying population.

The distributions of dust attenuations for the LAE and non-LAE samples differ significantly, with a median  $E(B-V)$  of 0.13 for the LAEs and 0.20 for the non-LAEs. While both populations have roughly the same distribution of  $E(B-V)$  values below 0.30, the non-LAE distribution is characterized by a tail of high extinction values. No LAEs have  $E(B-V) > 0.40$ , whereas 12/145 (8%) of non-LAEs do. The K-S test probability that the LAE and non-LAE extinction distributions derive from the same parent population is  $\sim 2\%$ .

The star formation rates of LAEs and non-LAEs are markedly different, as the LAEs have a median rate of  $25 M_\odot \text{ yr}^{-1}$  and the non-LAEs are characterized by a median rate of  $59 M_\odot \text{ yr}^{-1}$ . The relative quiescence of strong  $\text{Ly}\alpha$ -emitters is in contrast to the high SFR tail observed in non-LAEs, where star formation rates in excess of  $500 M_\odot \text{ yr}^{-1}$  are recorded for 22 objects<sup>10</sup>. There

<sup>10</sup> 15/22 of these objects, however, are younger than 10 Myr. While these objects have unphysically young ages (given that the

is a  $\sim 1\%$  probability of these LAE and non-LAE star formation rate distributions are drawn from the same underlying population.

Unlike age,  $E(B-V)$ , and SFR, the stellar mass distributions of LAEs and non-LAEs are not strongly dissimilar. The median value of the LAEs ( $1.1 \times 10^{10} M_\odot$ ) is only 40% larger than that of the non-LAEs ( $7.9 \times 10^9 M_\odot$ ) and a K-S test predicts that the two distributions have a  $\sim 27\%$  chance of being drawn from the same parent distribution.

We have shown that three of the best-fit stellar population parameters – age,  $E(B-V)$ , and SFR – have markedly different distributions in the LAE and non-LAE samples. LAEs are typically older, less dusty, and less vigorously forming stars than non-LAEs. We tested the robustness of these results by constructing bootstrap samples from the confidence intervals of best-fit stellar parameters (§4.2). The mean and the error on the mean ( $\sigma/\sqrt{n}$ , where  $n$  is the sample size) were calculated for each best-fit stellar population parameter in the LAE and non-LAE samples. This process was repeated for 100 bootstrap samples (Figure 11). For  $E(B-V)$ , age, and SFR, we found that the means of the LAE and non-LAE samples were consistently offset by at least their errors. In terms of stellar mass, the LAEs samples had consistently larger values; we note, however, that the masses of the LAE and non-LAE samples were comparable within their errors. These results, in agreement with the histograms discussed above, support the observed correlation that galaxies with strong Ly $\alpha$  emission tend to be older, less dusty, and more quiescent than objects with weak Ly $\alpha$  emission, or the line in absorption.

#### 4.4. Spectral Energy Distributions

In order to place the results of the previous section on a more empirical footing, we transition here from focusing on stellar parameters and instead examine more broadly the relative colors of objects with and without strong Ly $\alpha$  emission. We also contrast our data with SEDs of narrowband-selected LAEs from Gawiser et al. (2007) and Nilsson et al. (2007) with the aim of investigating the color differences, if any, between objects isolated with color cuts and narrowband filters. Our analysis is focused on the 179 objects in the LBG sample satisfying the criteria of population synthesis modeling and no  $K_s$  upper limits. This empirical approach is complementary to the stellar population modeling discussed previously, and is furthermore a non-parametric probe of the differences between objects with and without strong Ly $\alpha$  emission. Such a study is necessary given the well-known degeneracies among physical properties (e.g., dust extinction and age) derived from stellar population modeling (Shapley et al. 2003).

We find stark differences between the colors of LAEs and non-LAEs (Table 3), where all  $G$  magnitudes have been corrected for the contribution of Ly $\alpha$  (§3). Strong Ly $\alpha$ -emitters have bluer  $G - \mathcal{R}$  colors than non-LAEs ( $\langle G - \mathcal{R} \rangle_{\text{LAE}} = 0.54$ ;  $\langle G - \mathcal{R} \rangle_{\text{non-LAE}} = 0.65$ ) and this trend is consistent when a correction for IGM absorption (Madau 1995) is applied to the objects'  $G$  magnitudes

dynamical timescale of LBGs is  $\geq 10$  Myr; Giavalisco et al. 1996; Pettini et al. 1998, 2001), re-modeling these galaxies with the constraint that  $t_\star \geq 10$  Myr still results in best-fit star formation rates of several hundred  $M_\odot \text{ yr}^{-1}$ .

TABLE 3  
AVERAGE PHOTOMETRY\*

Sample ( $\langle z \rangle$ )	$\langle \mathcal{R} \rangle$ ( $\sigma$ )	$\langle G \rangle^a$ ( $\sigma$ )	$\langle G_{\text{IGM corr.}} \rangle$ ( $\sigma$ )	$\langle K_s \rangle^b$
LAEs (2.99)	24.31 (0.02)	24.85 (0.03)	24.67 (0.03)	21.24
non-LAEs (2.97)	24.34 (0.01)	24.99 (0.01)	24.81 (0.01)	21.36

\*Galaxies with  $K_s$  upper limits were omitted from this analysis, as were objects lacking stellar population modeling.

<sup>a</sup> $G$  magnitudes have been corrected to account for contributions from Ly $\alpha$ .

<sup>b</sup>Photometry calculated from best-fit SED, for objects lacking  $K_s$  imaging.

( $\langle G_{\text{IGM corr.}} - \mathcal{R} \rangle_{\text{LAE}} = 0.36$ ;  $\langle G_{\text{IGM corr.}} - \mathcal{R} \rangle_{\text{non-LAE}} = 0.47$ ). Given that non-LAEs have younger best-fit stellar ages than LAEs (§4.2), we expect that non-LAEs should have intrinsically bluer stellar continua than objects with strong Ly $\alpha$  emission. The fact that we instead observe redder  $G - \mathcal{R}$  colors in these objects is evidence that non-LAEs are more strongly attenuated by dust than LAEs. This result is consistent with the larger  $E(B-V)$  values derived for the non-LAEs than the LAEs (§4.2).

LAEs and non-LAEs also differ in their  $\mathcal{R} - K_s$  colors, where  $K_s$  magnitudes were inferred from best-fit SEDs for the 78 objects lacking near-infrared photometry. We find that LAEs are characterized by  $\langle \mathcal{R} - K_s \rangle = 3.07$ , whereas non-LAEs are bluer by 0.1 magnitudes with  $\langle \mathcal{R} - K_s \rangle = 2.98$ . Given that the  $\mathcal{R}$  and  $K_s$  passbands bracket the Balmer break for objects at  $z \sim 3$ , a redder  $\mathcal{R} - K_s$  color is indicative of a larger Balmer break. A more pronounced Balmer break, in turn, is correlated with an older stellar population (e.g., Bruzual & Charlot 2003). Therefore, the result that LAEs have redder  $\mathcal{R} - K_s$  colors than non-LAEs is empirical, non-parametric evidence that strong Ly $\alpha$ -emitters are older on average. We have accordingly shown that the different colors of LAEs and non-LAEs are reflective of the trends discerned using stellar population modeling.

Composite best-fit SEDs of the LAE and non-LAE samples were assembled by directly summing the individual best-fit SEDs over the rest frame range 912 Å–1.0  $\mu\text{m}$  and normalizing by the number of constituent spectra (34 and 145, respectively). In Figure 12, we compare the composite LAE and non-LAE spectra with best-fit average SEDs from two studies of narrowband-selected LAEs. Data from Nilsson et al. (2007) and Gawiser et al. (2007), where the former include LAEs at  $z \sim 3.1$  in the GOODS South Field and the latter encompass LAEs at  $z \sim 3.1$  in the Extended Chandra Deep Field South, are shown both normalized and un-normalized with our LAE and non-LAE composite spectra. It is immediately apparent that the LBG-selected LAEs and non-LAEs are significantly brighter than the narrowband-selected LAEs ( $\sim \times 2.3$  magnitudes in the  $\mathcal{R}$  band). The LBG-selected objects also have redder  $G - \mathcal{R}$  and redder  $\mathcal{R} - K_s$  colors than both the Nilsson et al. (2007) and Gawiser et al. (2007) data. These differences in color are consistent with LBG-selected objects being both dustier and older than objects isolated with narrowband filters, as has been suggested by some authors (e.g., Gawiser et al. 2007; Nilsson et al. 2008). The relationship between LBGs and narrowband-selected LAEs is far from clear, though; some authors hypothesize a continuity between at least portions of the two populations based on similari-



ties in stellar mass, color, and clustering (e.g., Adelberger et al. 2005b; Gronwall et al. 2007; Gawiser et al. 2007; Lai et al. 2008; Verhamme et al. 2008) whereas others maintain that the large luminosity and  $W_{\text{Ly}\alpha}$  discrepancies between LBGs and objects isolated with narrowband filters dictate separate evolutionary paths (e.g., Malhotra & Rhoads 2002).

## 5. DISCUSSION

Our large data set of both spectroscopically-determined Ly $\alpha$  equivalent widths and stellar population parameters constitutes a unique sample with which to investigate some of the current trends reported for continuum- and narrowband-selected objects. We turn here to examining several of the outstanding questions pertaining to LBGs and narrowband-isolated LAEs, with the constant aim of physically motivating our work. We begin below with a discussion of the necessity of comparing objects drawn from the same parent luminosity distribution.

### 5.1. A Caveat: Differing Rest-Frame Luminosities

By virtue of broadband selection techniques, LBGs have characteristically brighter optical continua than narrowband-selected LAEs ( $\mathcal{R} \leq 25.5$  versus  $R \sim 27$ ). As it is critical to disentangle how luminosity and stellar populations are related before attributing galaxy differences purely to the same mechanisms that modulate Ly $\alpha$  emission, it is of interest to investigate how, if at all, the derived properties of narrowband-selected LAEs are a natural result of preferentially isolating continuum-faint, line-bright objects. We compare our data with the work of several authors to explore the dependencies of Ly $\alpha$  emission, stellar populations, and spatial clustering on broadband luminosity and we discuss the applications of such investigations to both LBGs and narrowband-selected LAEs.

*Luminosity and Equivalent Width:* Recent work has suggested a correlation between luminosity and Ly $\alpha$  equivalent width, in the sense that few luminous LBGs have been observed with large equivalent widths (e.g., Shapley et al. 2003; Erb et al. 2006a; Ando et al. 2006; Ouchi et al. 2008; Vanzella et al. 2009; Pentericci et al. 2009). Several physical pictures have been suggested to explain this correlation, which has been noted in samples at redshifts  $z \sim 3$ –6. Verhamme et al. (2008) and Vanzella et al. (2009) hypothesized that different dust attenuations (from a luminosity-dependent chemical evolution history) could be responsible while Ando et al. (2006) suggested that an enhanced presence of HI gas around luminous LBGs could explain the lack of large Ly $\alpha$  equivalent widths in bright galaxies (consistent with the prediction of more massive galaxies residing in larger dark matter halos that are presumably richer in HI gas). Some authors, however, have conversely reported that the correlation between luminosity and Ly $\alpha$  equivalent width is tenuous, at best (e.g., Steidel et al. 2000; Verma et al. 2007; Stanway et al. 2007; Nilsson et al. 2009a). Given the ongoing debate about such a correlation, we examined our extensive data set to test for a deficiency of luminous objects with large Ly $\alpha$  equivalent widths.

We restricted our analysis to the 64 objects with  $W_{\text{Ly}\alpha} \geq 20 \text{ \AA}$  in order to ensure completeness as a function of

$\mathcal{R}$  magnitude, given that spectroscopic follow-up is biased toward objects with large, positive Ly $\alpha$  equivalent widths. These objects have  $W_{\text{Ly}\alpha} < 160 \text{ \AA}$  and  $M_{\text{UV}}$  ranging from  $-20.0$  to  $-22.4$  (neglecting corrections for dust attenuation). This parameter space is comparable to that of Ando et al. (2006), where these authors suggest a threshold luminosity of  $M_{1400} = -21.5$  to  $-21.0$  above which objects are deficient in large  $W_{\text{Ly}\alpha}$  values. We find that  $M_{\text{UV}}$  and  $W_{\text{Ly}\alpha}$  are not correlated in our sample, where the Spearman  $\rho$  test statistic,  $r_{\text{SR}}$ , is  $-0.104$  and the probability of a null hypothesis,  $P_{\text{SR}}$ , is  $0.4076$ . Furthermore, we see no evidence for any such threshold luminosity in our data; when the sample is divided into bright ( $M_{\text{UV}} < -21.0$ ) and faint ( $M_{\text{UV}} > -21.0$ ) groups, the median  $W_{\text{Ly}\alpha}$  of each group are identical ( $\sim 32 \text{ \AA}$ ).

These results are contradictory to those presented by Shapley et al. (2003) who also examined a sample of  $z \sim 3$  LBGs. The Shapley et al. (2003) sample, when limited to objects with  $W_{\text{Ly}\alpha} \geq 20 \text{ \AA}$ , consisted of objects with absolute UV luminosities between  $-19.5$  and  $-22.4$  (neglecting corrections for dust attenuation). In those data, there is a significant correlation between  $M_{\text{UV}}$  and  $W_{\text{Ly}\alpha}$  ( $r_{\text{SR}} = 0.274$ ;  $P_{\text{SR}} = 0.0002$ ). Dividing this sample into bright and faint subgroups, where the boundary luminosity is  $M_{\text{UV}} = -21.0$ , also yielded a pronounced difference in the median  $W_{\text{Ly}\alpha}$  values of each group:  $M_{\text{UV}}(\text{bright}) = 35 \text{ \AA}$  and  $M_{\text{UV}}(\text{faint}) = 44 \text{ \AA}$ . Given that both our present sample and the Shapley et al. (2003) sample are composed of  $z \sim 3$  LBGs, we hypothesize that one of reasons our data may not exhibit a correlation between  $M_{\text{UV}}$  and  $W_{\text{Ly}\alpha}$  is that our sample includes only a limited number of high equivalent width objects. Nine objects have  $W_{\text{Ly}\alpha} \geq 70 \text{ \AA}$  and just one has  $W_{\text{Ly}\alpha} \geq 100 \text{ \AA}$  in our data set whereas, in the Shapley et al. (2003) sample, 45 objects have  $W_{\text{Ly}\alpha} \geq 70 \text{ \AA}$  and 20 have  $W_{\text{Ly}\alpha} \geq 100 \text{ \AA}$ . After testing that our systematic approach to calculating Ly $\alpha$  equivalent width returned values consistent with those reported by Shapley et al. (2003), we combined our data with the 189 objects<sup>11</sup> from Shapley et al. (2003) with  $W_{\text{Ly}\alpha} \geq 20 \text{ \AA}$ . This combined sample of 243 objects, with equivalent widths measured in a uniform manner, was then tested for a correlation between  $M_{\text{UV}}$  and  $W_{\text{Ly}\alpha}$ . We found only a moderate correlation ( $r_{\text{SR}} = 0.149$ ;  $P_{\text{SR}} = 0.0202$ ), where we hypothesize that the trend between  $M_{\text{UV}}$  and  $W_{\text{Ly}\alpha}$  is simply not strong enough to be unequivocally detected in all samples. Furthermore, the correlation between  $M_{\text{UV}}$  and  $W_{\text{Ly}\alpha}$  in these data may be masked by the relatively small range of  $M_{\text{UV}}$  probed by LBGs. Narrowband-selected LAEs exhibit a wider range of absolute luminosities ( $23.0 \lesssim R \lesssim 27.0$ ) than LBGs do ( $23.0 \lesssim \mathcal{R} \lesssim 25.5$ ); any trend between  $M_{\text{UV}}$  and  $W_{\text{Ly}\alpha}$  will consequently be more pronounced in a sample of LAEs. In order to test this statement, we analyzed a sample of LAEs from Gronwall et al. (2007). We divided the data into two samples, where the first subsample included only objects brighter than the LBG spectroscopic limit and the second subsample was inclusive of all the data. The first subsample showed

<sup>11</sup> We limit our analysis to the 179/189 galaxies satisfying the criterion  $W_{\text{Ly}\alpha} \geq 20 \text{ \AA}$ , measured according to our methodology described in §2.3; 10 objects classified as LAEs in the Shapley et al. (2003) sample do not have equivalent widths above  $20 \text{ \AA}$  when measured using our systematic technique.

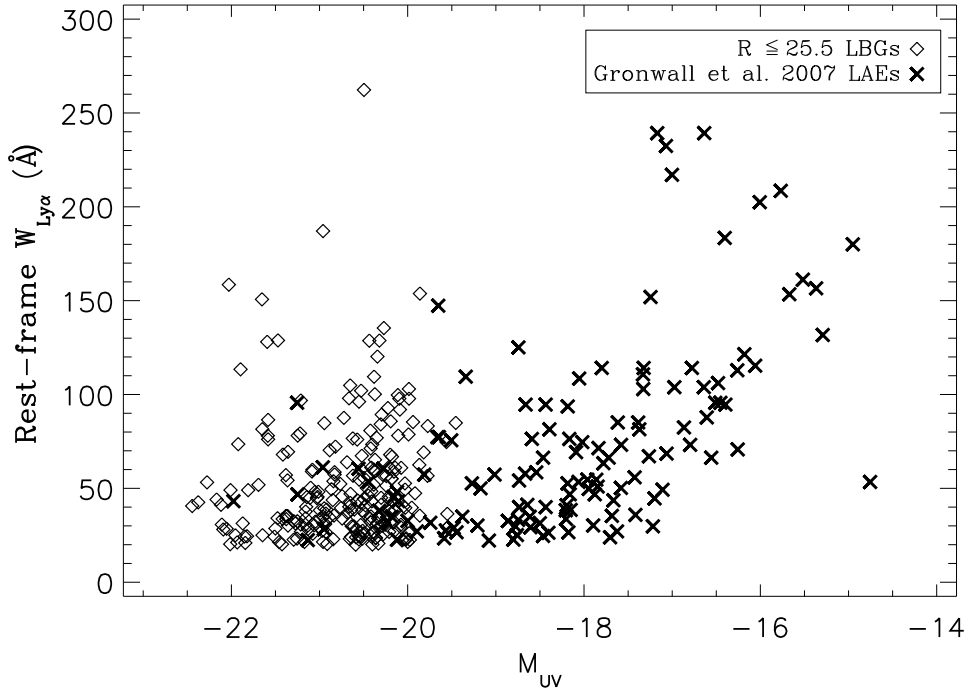


FIG. 13.— Absolute UV magnitude versus rest-frame  $W_{\text{Ly}\alpha}$  for  $\mathcal{R} \leq 25.5$  LBGs (diamonds) and the Gronwall et al. (2007) sample of  $z = 3.1$  LAEs (crosses). A strong correlation between  $M_{\text{UV}}$  and  $W_{\text{Ly}\alpha}$  is observed in the Gronwall et al. (2007) sample while weaker correlations are seen in the sample of  $z \sim 3$  LBGs. We attribute this discrepancy to the larger range of  $M_{\text{UV}}$  probed by LAEs.

no correlation between  $M_{\text{UV}}$  and  $W_{\text{Ly}\alpha}$  ( $r_{\text{SR}} = -0.015$ ;  $P_{\text{SR}} = 0.9185$ ) whereas the second subsample exhibited a strong correlation ( $r_{\text{SR}} = 0.585$ ;  $P_{\text{SR}} = 0.0000$ ). These results support our hypothesis that the trend between  $M_{\text{UV}}$  and  $W_{\text{Ly}\alpha}$  at  $z \sim 3$  is apparent only when considering data encompassing a large range in absolute luminosity. In Figure 13, we present a plot of  $M_{\text{UV}}$  versus  $W_{\text{Ly}\alpha}$  for  $\mathcal{R} \leq 25.5$  LBGs and the Gronwall et al. (2007) sample of narrowband-selected LAEs. Even if one assumes incompleteness in the Gronwall et al. (2007) sample at the faint end, the lack of large equivalent widths among bright objects is striking.

**Luminosity and Stellar Populations:** Understanding how luminosity and stellar populations are correlated is critical to commenting on the nature of LBGs and LAEs, given that the latter are commonly an order of magnitude fainter in optical broadband filters. Lai et al. (2008) examined a sample of 70  $z \sim 3.1$  LAEs,  $\sim 30\%$  of which were detected in the *Spitzer* IRAC 3.6  $\mu\text{m}$  band. These authors found that the IRAC-detected LAEs were significantly older and more massive ( $\langle t_{\star} \rangle \sim 1.6$  Gyr,  $\langle M \rangle \sim 9 \times 10^9 M_{\odot}$ ) than the IRAC-undetected sample ( $\langle t_{\star} \rangle \sim 200$  Myr,  $\langle M \rangle \sim 3 \times 10^8 M_{\odot}$ ). In addition to having redder colors, the IRAC-detected sample was also approximately three times brighter in the  $R$  band. This correlation between luminosity and redness, age, and mass prompted Lai et al. (2008) to suggest that the IRAC-detected LAEs may be a low-mass extension of the LBG population. The relationship between luminosity and average dust attenuation was examined by Reddy et al. (2008), where these authors studied a sample of UV-selected objects at  $1.9 \leq z < 3.4$  and found no correlation between  $M_{\text{UV}}$  and  $E(B-V)$  over the absolute magnitude range  $22.0 \leq \mathcal{R} \leq 25.5$ . While bright objects

do not appear to exhibit a correlation between dust attenuation and luminosity, Reddy et al. (2008) postulate that objects fainter than the LBG spectroscopic limit of  $\mathcal{R} = 25.5$  may have lower average dust attenuations than brighter objects. This has been confirmed by Bouwens et al. (2009), who examined a sample of objects at  $z \sim 2-6$  over a larger dynamic range ( $0.1L_{z=3}^*$  to  $2L_{z=3}^*$ ) than had been previously studied. These authors reported a correlation between UV luminosity and dust attenuation such that fainter objects are bluer. Given the correlation we find between  $E(B-V)$  and  $W_{\text{Ly}\alpha}$ , the evolution of dust attenuation with UV luminosity may have implications for the fraction of LAEs as a function of UV luminosity (Reddy & Steidel 2009). These results have highlighted that examining objects over only a limited range of absolute magnitudes may mask an underlying correlation.

**Luminosity and Clustering:** Several authors have noted the different clustering properties of LBGs and LAEs, where the former exhibit a mean halo occupation of  $\sim 100\%$  (e.g., Conroy et al. 2008) in dark matter halos with minimum masses of  $\sim 10^{11.3} h^{-1} M_{\odot}$  (e.g., Adelberger et al. 2005b; Conroy et al. 2008) and the latter cluster more weakly and appear to occupy only  $1/100 - 1/10$  of similarly-clustered dark matter halos with lower limit masses of  $\sim 10^{10.6} h^{-1} M_{\odot}$  (e.g., Gawiser et al. 2007). Given the direct dependence of clustering strength on UV luminosity (e.g., Ouchi et al. 2004; Adelberger et al. 2005b; Lee et al. 2006), the spatial differences between LBGs and LAEs may simply reflect the discrepancy in typical UV luminosity between the two samples. It is therefore of interest to investigate how the clustering strength of LAEs correlates with  $\text{Ly}\alpha$  luminosity or  $\text{Ly}\alpha$  equivalent width, given that these quantities

govern the selection of LAEs. Discerning the relative clustering properties of objects with and without strong Ly $\alpha$  emission *within the same UV luminosity range* is critical to understanding the correlation between Ly $\alpha$  and galactic properties.

These results – that objects more luminous in the rest-frame UV may 1) be deficient in large Ly $\alpha$  equivalent widths and 2) be generally redder, older, and more massive relative to less luminous objects – may be the driving factors responsible for (faint, high equivalent width) narrowband-selected LAEs being typically younger, bluer, and less massive than (bright, lower equivalent width) LBGs.

As the LBG spectroscopic limit of  $\mathcal{R} \leq 25.5$  necessarily limits our sample to a smaller absolute magnitude range than than probed by narrowband-selected LAEs ( $23.0 \lesssim R \lesssim 27.0$ ), the luminosity-dependent trends reported above for Ly $\alpha$  equivalent width, stellar populations, and clustering (e.g., Ando et al. 2006; Lai et al. 2008; Adelberger et al. 2005b) may only become apparent in narrowband-selected samples where the absolute luminosity range is significantly larger than it is in samples of LBGs. We remind the reader that while our conclusions are applicable to both LBGs and bright ( $\mathcal{R} \leq 25.5$ ) narrowband-selected LAEs, we are unable to make inferences about the population of faint LAEs. We refer the reader to Lai et al. (2008) for a discussion of these objects.

### 5.2. LBG and LAE Equivalent Width Distributions

The equivalent width of the Ly $\alpha$  feature is a common benchmark that can be used to make comparisons between studies of LBGs and LAEs. Observing programs of flux-selected Ly $\alpha$ -emitters typically employ a narrowband ( $\sim 50$ – $100$  Å) filter centered on the redshifted Ly $\alpha$  line, paired with a broadband filter used to characterize the local continuum. Samples are defined according to a minimum Ly $\alpha$  equivalent width – typically  $\sim 20$  Å in the rest frame – where  $W_{\text{Ly}\alpha}$  is calculated photometrically by ratioing the flux in the narrowband filter to the flux density in the broadband filter. LBGs, on the other hand, are selected according to broadband flux and color cuts, with no implicit requirement on  $W_{\text{Ly}\alpha}$ . Equivalent widths of LBGs are most commonly calculated spectroscopically, as these objects are characterized by relatively bright continua ( $\mathcal{R} \leq 25.5$ ). Given these different selection techniques and methods of calculating  $W_{\text{Ly}\alpha}$ , it is of interest to compare the equivalent width distributions of LBG-selected LAEs and narrowband-selected LAEs. A difference in the  $W_{\text{Ly}\alpha}$  distributions of these two populations would be indicative of an underlying dissimilarity between LBG-selected LAEs and narrowband-selected LAEs, even though both classes of objects can be broadly classified as strong Ly $\alpha$ -emitters<sup>12</sup>.

For this analysis, we combined our present sample of 64 LBG-selected LAEs with the 179 objects from Shapley et al. (2003) satisfying the criterion of  $W_{\text{Ly}\alpha} \geq 20$

(measured using our methodology described in §2.3). Integrating these two data sets yields a large sample of  $z \sim 3$  objects for which equivalent widths were measured in an identical manner. We find that these data are characterized by a median equivalent width of 42 Å and mean of 57 Å. In contrast, a sample of 160 LAEs at  $z = 3.1$  in the Extended Chandra Deep Field South observed by Gronwall et al. (2007) had a median of  $\sim 60$  Å and a mean of  $\sim 80$  Å. We used the K–S test to quantify the likelihood that the LBG-selected LAEs and the narrowband-selected LAEs derived from the same parent equivalent width distribution. When the entire sample of objects from Gronwall et al. (2007) was considered, we found a probability of  $3.5 \times 10^{-4}$  that the objects shared a common equivalent width distribution. Alternatively, when we limited the Gronwall et al. (2007) data to include only objects satisfying the LBG spectroscopic limit of  $\mathcal{R} \leq 25.5$ , we obtained a probability of  $\sim 0.95$  that the equivalent widths of the LBG- and narrowband-selected LAE samples could be described as originating from the same population. This result, consistent with Verhamme et al. (2008), is indicative of the similarity in equivalent width of objects spanning comparable UV luminosities. Conversely, the probability that the equivalent widths of our sample of LBG-selected LAEs and the faint ( $R \geq 25.5$ ) Gronwall et al. (2007) LAEs derive from the same parent population is  $8 \times 10^{-8}$ . Similarly, when the Gronwall et al. (2007) data are divided using the boundary  $R = 25.5$ , a K–S test yields a probability of  $7.9 \times 10^{-6}$  that the two equivalent width populations derive from the same parent distribution.

In other words, while the equivalent width distributions of LBG- and narrowband-selected LAEs are quite disparate when considered at face value, it appears that the bulk of this disparity can be attributed to the different luminosities probed by the respective samples. When narrowband-selected LAEs are restricted to objects more luminous than  $R = 25.5$ , a K–S test reveals a high probability that the equivalent width distributions of strong Ly $\alpha$ -emitting LBGs and bright LAEs derive from the same parent population. This similarity in equivalent width, when a standard continuum magnitude range is adopted, is consistent with the picture that bright LAEs represent the same population as Ly $\alpha$ -emitting LBGs (e.g., Verhamme et al. 2008).

### 5.3. Escape of Ly $\alpha$ Photons

As Ly $\alpha$  is susceptible to a variety of complex radiation transport effects including resonant scattering (e.g., Neufeld 1990) and the velocity field of the ISM (e.g., Verhamme et al. 2008), the escape of Ly $\alpha$  emission is a probe of the physical conditions of galaxies’ interstellar media. In the simplest case of a single-phase ISM in which gas and dust are well mixed, Ly $\alpha$  photons experience more attenuation than continuum photons due to the longer dust absorption path lengths expected for resonantly scattered radiation. To explain the large Ly $\alpha$  equivalent widths observed in some apparently dusty LAEs, the presence of a multi-phase ISM – in which dust is segregated in neutral clouds – has been proposed (Neufeld 1991; Hansen & Oh 2006; Finkelstein et al. 2009). In such a geometry, Ly $\alpha$  photons are scattered at the surface of dusty clumps while continuum photons penetrate the clumps and are preferentially scattered or absorbed.

<sup>12</sup> Reddy et al. (2008) found that the standard LBG color selection criteria (Equation 1) do little to bias the intrinsic distribution of  $W_{\text{Ly}\alpha}$  for  $z \sim 3$  LBGs, given the low probability of an object having a strong enough Ly $\alpha$  feature to perturb its colors out of the LBG selection window. We therefore attribute any differences in the  $W_{\text{Ly}\alpha}$  distributions of LBGs and narrowband-selected LAEs to intrinsic dissimilarities between the two populations.

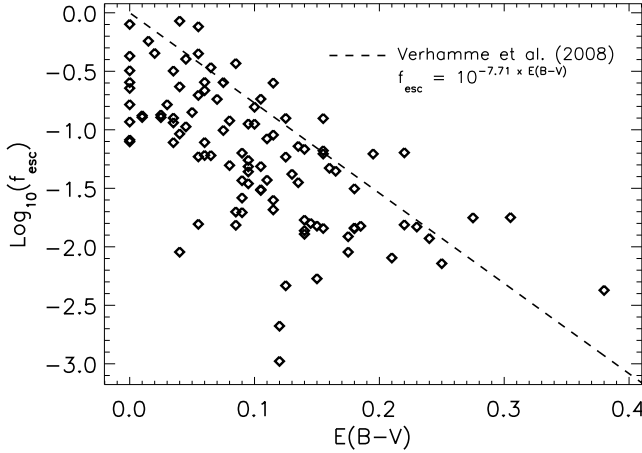


FIG. 14.—  $\text{Ly}\alpha$  escape fraction as a function of dust extinction, for objects with best-fit stellar ages  $t_\star > 100$  Myr. A significant correlation is observed, in the sense that objects with lower dust attenuations have larger escape fractions. The best-fit line from Verhamme et al. (2008) is overplotted as a dashed line.

Galaxies in which the dust is segregated in neutral clouds are consequently predicted to exhibit larger  $\text{Ly}\alpha$  equivalent widths than would be expected given their stellar populations.

We considered the likelihood of the above dust geometry in our sample of LBGs. Our methodology relied on comparing observed and predicted  $\text{Ly}\alpha$  luminosities, where the former,  $L_{\text{Ly}\alpha(\text{flux})}$ , was calculated simply from the  $\text{Ly}\alpha$  line flux and the latter,  $L_{\text{Ly}\alpha(\text{SFR})}$ , was derived from the conversion between SFR (from population synthesis modeling) and  $\text{Ly}\alpha$  luminosity, assuming the conventions (Case B recombination;  $T_e = 10,000$  K) of Kennicutt (1998) and Brocklehurst (1971):

$$L_{\text{Ly}\alpha(\text{SFR})} = \frac{\text{SFR} [M_\odot \text{ yr}^{-1}]}{9.1 \times 10^{-43}} \quad (2)$$

where SFR was calculated assuming a Salpeter (1955) IMF. Two similar parameters incorporating observed and predicted  $\text{Ly}\alpha$  luminosities were of interest: the escape fraction,  $f_{\text{esc}}$ , and the relative escape fraction,  $f_{\text{esc,rel}}$ . The escape fraction is the ratio of observed to predicted  $\text{Ly}\alpha$  luminosities, whereas the relative escape fraction is this same ratio with an extra term corresponding to a dust correction at the rest wavelength of  $\text{Ly}\alpha$ .  $f_{\text{esc,rel}}$  is a probe of the degree to which  $\text{Ly}\alpha$  and continuum photons experience the same level of dust attenuation. In the case that  $f_{\text{esc,rel}} = 1$ ,  $\text{Ly}\alpha$  and continuum photons are attenuated by the same  $E(B-V)$ . On the other hand, a relative escape fraction less than unity is indicative of a dust geometry in which  $\text{Ly}\alpha$  photons are attenuated more than continuum photons. Conversely, a galaxy in which dust is segregated in neutral clouds and where the  $\text{Ly}\alpha$  flux is consequently enhanced relative to the continuum flux would have  $f_{\text{esc,rel}} > 1$ . We present the equations for  $f_{\text{esc}}$  and  $f_{\text{esc,rel}}$  below, where  $k'(1216)$  parameterizes the Calzetti et al. (2000) starburst attenuation law at 1216 Å:

$$f_{\text{esc}} = \frac{L_{\text{Ly}\alpha(\text{flux})}}{L_{\text{Ly}\alpha(\text{SFR})}}, \quad (3)$$

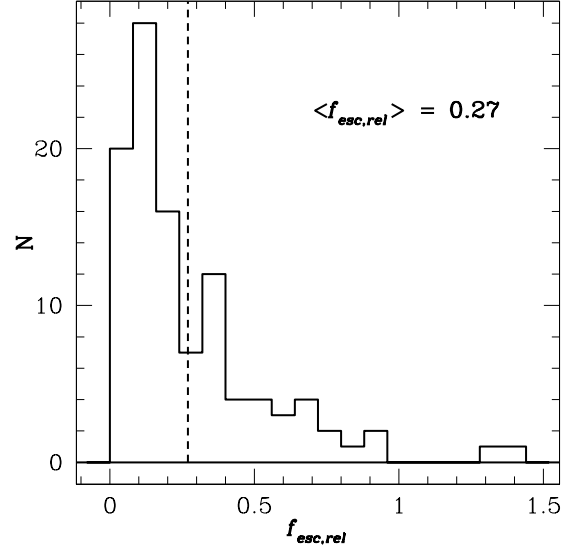


FIG. 15.— Histogram of  $f_{\text{esc,rel}}$  values, for objects with  $t_\star > 100$  Myr. Note that the majority of objects (103/105) have  $f_{\text{esc,rel}} < 1$ , where the sample as a whole is characterized by  $\langle f_{\text{esc,rel}} \rangle = 0.27$ . These low relative escape fractions are indicative of  $\text{Ly}\alpha$  photons experiencing more attenuation than non-resonance continuum photons. These results are not consistent with the hypothesis of a clumpy interstellar medium, as has been suggested to exist in some LAEs (e.g., Finkelstein et al. 2009).

$$f_{\text{esc,rel}} = f_{\text{esc}} \times 10^{0.4E(B-V)k'(1216)}. \quad (4)$$

When calculating  $f_{\text{esc}}$  and  $f_{\text{esc,rel}}$ , we limited our analysis to only those objects with  $W_{\text{Ly}\alpha} > 0$  Å due to the unphysical nature of inferring a  $\text{Ly}\alpha$  luminosity from a negative  $\text{Ly}\alpha$  flux. We also required objects to have best-fit stellar ages older than 100 Myr in order to ensure the validity of Equation 2, which assumes continuous star formation for at least that duration (Kennicutt 1998). These criteria isolated a sample of 105 objects. We note that the questions raised about the nature of the dust extinction law for young objects (§4.2) are not of concern given this older sample. To correct for slit losses, we normalized the  $G$  magnitudes determined from photometry and spectroscopy; the latter were calculated by multiplying the  $G$  filter transmission curve (4780/1100 Å) over the optical spectra. The  $\text{Ly}\alpha$  line fluxes were adjusted accordingly, where the median flux correction was an increase by a factor of  $\sim 1.7$  (0.6 magnitudes). This procedure relies on the assumption that  $\text{Ly}\alpha$  emission has the same spatial extent as broadband 940–1470 Å emission. While some recent work (e.g., Steidel et al. 2000; Matsuda et al. 2004; Hayashino et al. 2004) has suggested that  $\text{Ly}\alpha$  and UV continuum emission may be spatially decoupled with  $\text{Ly}\alpha$  more extended than continuum emission, in the absence of simultaneous high-resolution  $\text{Ly}\alpha$  and UV continuum imaging for our entire sample we assume for simplicity that the line and continuum emission are coincident.

The calculated values of  $f_{\text{esc}}$  vary from 0.00–0.85. Gronwall et al. (2007) and Nilsson et al. (2009b) report typical  $f_{\text{esc}}$  values of  $\sim 0.30$  and  $\sim 0.60$  in LAE samples at  $z \sim 3.1$  and  $z \sim 2.25$ , respectively. In Figure 14, we plot  $E(B-V)$  versus  $f_{\text{esc}}$ ; we find a strong correlation in the sense that objects with large dust attenuations tend

to have small Ly $\alpha$  escape fractions ( $r_{\text{SR}} = -0.712$ ,  $P_{\text{SR}} = 0.0000$ ). We note that this trend is consistent with the existence of LBGs in our sample exhibiting both Ly $\alpha$  in absorption and red UV continua, where these particular objects were not included in this analysis due to their negative Ly $\alpha$  fluxes. Other authors have derived similar results, although with significantly smaller sample sizes (e.g., Verhamme et al. 2008; Atek et al. 2009). The scatter present in our larger data set – some of which may be due to systematics in estimating  $f_{\text{esc}}$  – is a useful probe of the nature of Ly $\alpha$  radiative transfer in LBGs. We further discuss a physical picture of LBGs consistent with these  $f_{\text{esc}}$  results in §6.

In order to investigate the nature of the gas and dust distributions for the objects in our sample, we derived the relative escape fraction of the 105 LBGs with  $W_{\text{Ly}\alpha} > 0 \text{ \AA}$  and  $t_{\star} > 100 \text{ Myr}$ . We found that 103 objects had  $f_{\text{esc,rel}} < 1$  and the sample as a whole was characterized by  $\langle f_{\text{esc,rel}} \rangle = 0.27$  (Figure 15). Even if we conservatively assume Ly $\alpha$  slit losses approaching a factor of two (Hayashino et al. 2004), these low relative escape fractions, well below unity, do not support the hypothesis in which dust is primarily segregated to neutral clouds in Ly $\alpha$ -emitting LBGs. Rather, Ly $\alpha$  appears to experience more attenuation than continuum photons, consistent with the physical picture of a homogeneous distribution of gas and dust in which resonantly scattered Ly $\alpha$  photons have longer dust absorption path lengths than continuum photons. Such a simple picture is likely not an accurate representation of the ISM of  $z \sim 3$  LBGs; indeed, the ISM of our own Milky Way is known to be highly inhomogeneous (Dickey & Garwood 1989). However, our results suggest a scenario in which dust and gas are well mixed among the different phases of an inhomogeneous ISM.

## 6. SUMMARY AND CONCLUSIONS

We have analyzed a sample of 321 optically-selected  $z \sim 3$  Lyman break galaxies in order to investigate the relationship between stellar populations and Ly $\alpha$  emission. The equivalent width of the Ly $\alpha$  feature was robustly estimated from rest-frame UV spectroscopy and broadband *GRJK<sub>s</sub>* + *Spitzer* IRAC photometry was used to conduct stellar population modeling to derive the key properties of age, extinction, star formation rate, and stellar mass for all objects with photometric coverage in at least one near- or mid-infrared passband ( $\sim 80\%$  of the sample). The limited luminosity range of LBGs enabled a controlled investigation of the nature of Ly $\alpha$  emission *within a sample of objects spanning similar luminosities*. Given the luminosity-dependent trends in Ly $\alpha$  equivalent width, stellar populations, and clustering (e.g., Gronwall et al. 2007; Lai et al. 2008; Adelberger et al. 2005b), this controlled study represents an improvement over previous work. We used a variety of statistical tests to analyze the correlation between Ly $\alpha$  emission and stellar populations in LBGs from the standpoint of comparing spectroscopic observations, photometric data, and best-fit stellar population parameters. The relative Ly $\alpha$  escape fraction was used to probe the relative distributions of gas and dust in the objects’ interstellar media. Below, we summarize our results.

- Ly $\alpha$  equivalent width is correlated with age, SFR,

and E(B–V), respectively, in the sense that galaxies with strong Ly $\alpha$  emission are older, more quiescent, and less dusty than their counterparts with weak or absent Ly $\alpha$  emission. Taking into account the uncertainties on the best-fit population parameters, the probability of a null hypothesis (i.e., no correlation) was excluded at the 3–5 $\sigma$  level for these relationships. We found that stellar mass was not significantly correlated with  $W_{\text{Ly}\alpha}$  – the null hypothesis could be excluded at only the  $\sim 1\sigma$  level. These results were consistently derived from several different analyses of the data, including correlation tests, composite spectra, and the binary division of the sample into LAEs ( $W_{\text{Ly}\alpha} \geq 20 \text{ \AA}$ ) and non-LAEs ( $W_{\text{Ly}\alpha} < 20 \text{ \AA}$ ).

- Analysis of the relative escape fraction of Ly $\alpha$  is consistent with Ly $\alpha$  photons experiencing more attenuation than non-resonance continuum photons. We also find that the Ly $\alpha$  escape fraction is strongly correlated with E(B–V), where galaxies with more dust attenuation also have lower escape fractions.

The observed correlations between Ly $\alpha$  emission and stellar populations are consistent with the physical picture proposed by Shapley et al. (2001), in which young, dusty LBGs experience vigorous outflows from supernovae and massive star winds. Shapley et al. (2003) reported evidence that both gas and dust are entrained in the outflows, evidence that these “superwinds” could tenably decrease a galaxy’s dust and gas covering fraction over several tens of Myr. While the more mature LBGs may have as much or more overall dust content than younger galaxies, the fact that these older objects ( $t_{\star} \gtrsim 100 \text{ Myr}$ ) are also more likely to exhibit Ly $\alpha$  emission is an important point: this trend demonstrates that it is the dust covering fraction – not the total amount of dust – that modulates Ly $\alpha$  emission. Independent evidence for a lower covering fraction of dusty gas in older objects is provided by a trend toward weaker low-ionization interstellar absorption lines with increasing age in the composite spectra presented in §4.2.

While this physical picture has been put forth previously, our current results are more strongly supported due to the wide range of statistical tests and analysis methods that we employed. We compared our larger sample of data in different forms – spectroscopic, photometric, and best-fit parameters – using a battery of statistical methods including correlation and K–S tests. Ly $\alpha$  emission strength was furthermore treated as both an independent and dependent variable. These analyses represent a systematic, powerful approach to elucidating trends.

Results of both the escape fraction and the relative escape fraction can be used to further constrain the physical picture of LBGs and bright narrowband-selected LAEs. While the observed inverse relationship between E(B–V) and  $f_{\text{esc}}$  is consistent with earlier results (e.g., Verhamme et al. 2008; Atek et al. 2009), the scatter present in our larger sample highlights the myriad factors modulating the Ly $\alpha$  escape fraction (e.g., galaxy kinematics, dust, and outflow geometry). Further analysis of this scatter will be instrumental in constraining how the

$\text{Ly}\alpha$  escape fraction varies. The observed relative escape fraction of  $\text{Ly}\alpha$  emission – where the majority of LBGs have  $f_{\text{esc,rel}}$  below unity – is indicative of a physical picture in which LBGs contain gas and dust that is well mixed. In this geometry,  $\text{Ly}\alpha$  photons experience more attenuation than continuum photons do because of the former’s increased path lengths from resonant scattering. This is in contrast to the scenario proposed by Finkelstein et al. (2009), in which dust is segregated in neutral gas clumps surrounded by an ionized, dust-free medium. We caution, however, that the relative escape fraction of  $\text{Ly}\alpha$  is likely modified by a variety of factors including galaxy kinematics, dust, and outflow geometry. As such, additional observations are necessary in order to more fully understand the distribution (and evolution) of gas and dust in LBGs.

While we hope that this work has illuminated the relationship between  $\text{Ly}\alpha$  emission and stellar populations in  $z \sim 3$  LBGs, future systematic studies at other redshifts – ideally over larger dynamic ranges in UV luminosity – are necessary in order to address the discrepancies between trends reported here and those at  $z \sim 2$  or  $z \sim 4$  (e.g., Erb et al. 2006a; Pentericci et al. 2007). The nature of complex  $\text{Ly}\alpha$  emission morphologies – such as the double-peaked objects that comprise  $\sim 4\%$  of the sample discussed here – has also yet to be explored in light of understanding if these objects’ stellar populations and gas distributions differ from those of more typical  $\text{Ly}\alpha$ -emitters or absorbers. Similarly, an analysis of the geometry of dust and gas in the interstellar media of  $z \sim 3$  LBGs is vital to understanding what kind of dust attenuation law – the Calzetti et al. (2000) relation, a SMC-like law, or another relation completely – most accurately describes these objects. Furthermore, a basic property critical to placing galaxies in an evolutionary context – metallicity – remains poorly constrained for

the  $z \sim 3$  LBG population (but see Maiolino et al. 2008). While metallicity has been investigated in the rare cases of gravitationally lensed objects (e.g., Teplitz et al. 2000; Pettini et al. 2002; Hainline et al. 2009; Quider et al. 2009), a systematic study of elemental abundances in a larger sample of  $z \sim 3$  LBGs would be illuminating (akin to the  $z \sim 2$  sample discussed in Erb et al. 2006a). Given anticipated advances in both telescopes and instrumentation, we hope that these questions are illustrative of many others that will help to guide future LBG research.

We thank Kim Nilsson and Eric Gawiser for kindly providing their data for comparison. A.E.S. acknowledges support from the David and Lucile Packard Foundation and the Alfred P. Sloan Foundation. D.K.E. is supported by a Spitzer Fellowship through a NASA grant administered by the Spitzer Science Center. C.C.S. has been supported by grants AST 03-07263 and AST 06-06912 from the National Science Foundation and by the David and Lucile Packard Foundation. Support for N.A.R. was provided by NASA through Hubble Fellowship grant HST-HF-01223.01 awarded by the Space Telescope Science Institute, which is operated by the Association of Universities for Research in Astronomy, Inc., for NASA, under contract NAS 5-26555. We also wish to recognize and acknowledge the very significant cultural role and reverence that the summit of Mauna Kea has always had within the indigenous Hawaiian community. We are most fortunate to have the opportunity to conduct observations from this mountain. This work is based in part on observations made with the *Spitzer Space Telescope*, which is operated by the Jet Propulsion Laboratory, California Institute of Technology under a contract with NASA.

## REFERENCES

- Adelberger, K. L., Shapley, A. E., Steidel, C. C., Pettini, M., Erb, D. K., & Reddy, N. A. 2005a, *ApJ*, 629, 636
- Adelberger, K. L., Steidel, C. C., Giavalisco, M., Dickinson, M., Pettini, M., & Kellogg, M. 1998, *ApJ*, 505, 18
- Adelberger, K. L., Steidel, C. C., Pettini, M., Shapley, A. E., Reddy, N. A., & Erb, D. K. 2005b, *ApJ*, 619, 697
- Adelberger, K. L., Steidel, C. C., Shapley, A. E., & Pettini, M. 2003, *ApJ*, 584, 45
- Ando, M., Ohta, K., Iwata, I., Akiyama, M., Aoki, K., & Tamura, N. 2006, *ApJ*, 645, L9
- Ando, M., Ohta, K., Iwata, I., Watanabe, C., Tamura, N., Akiyama, M., & Aoki, K. 2004, *ApJ*, 610, 635
- Atek, H., Kunth, D., Schaerer, D., Hayes, M., Deharveng, J.-M., Ostlin, G., & Mas-Hesse, J. M. 2009, *ArXiv e-prints*
- Bell, E. F., McIntosh, D. H., Katz, N., & Weinberg, M. D. 2003, *ApJS*, 149, 289
- Bouwens, R., Illingworth, G., Franx, M., Chary, R.-R., Meurer, G., Conselice, C., Ford, H., & Giavalisco, M. 2009, in preparation
- Bouwens, R. J., Illingworth, G. D., Franx, M., & Ford, H. 2008, *ApJ*, 686, 230
- Brocklehurst, M. 1971, *MNRAS*, 153, 471
- Bruzual, G., & Charlot, S. 2003, *MNRAS*, 344, 1000
- Calzetti, D., Armus, L., Bohlin, R. C., Kinney, A. L., Koornneef, J., & Storchi-Bergmann, T. 2000, *ApJ*, 533, 682
- Chabrier, G. 2003, *PASP*, 115, 763
- Chapman, S. C., Blain, A. W., Smail, I., & Ivison, R. J. 2005, *ApJ*, 622, 772
- Chapman, S. C., & Casey, C. M. 2009, *ArXiv e-prints*
- Cole, S., Lacey, C. G., Baugh, C. M., & Frenk, C. S. 2000, *MNRAS*, 319, 168
- Conroy, C., Shapley, A. E., Tinker, J. L., Santos, M. R., & Lemson, G. 2008, *ApJ*, 679, 1192
- Cowie, L. L., & Hu, E. M. 1998, *AJ*, 115, 1319
- Deharveng, J.-M., Small, T., Barlow, T. A., Péroux, C., Milliard, B., Friedman, P. G., Martin, D. C., Morrissey, P., Schiminovich, D., Forster, K., Seibert, M., Wyder, T. K., Bianchi, L., Donas, J., Heckman, T. M., Lee, Y.-W., Madore, B. F., Neff, S. G., Rich, R. M., Szalay, A. S., Welsh, B. Y., & Yi, S. K. 2008, *ApJ*, 680, 1072
- Dickey, J. M., & Garwood, R. W. 1989, *ApJ*, 341, 201
- Dickinson, M., Giavalisco, M., & The GOODS Team. 2003, in *The Mass of Galaxies at Low and High Redshift*, 324
- Diehl, R., Halloin, H., Kretschmer, K., Lichti, G. G., Schönfelder, V., Strong, A. W., von Kienlin, A., Wang, W., Jean, P., Knödseder, J., Roques, J.-P., Weidenspointner, G., Schanne, S., Hartmann, D. H., Winkler, C., & Wunderer, C. 2006, *Nature*, 439, 45
- Erb, D. K., Shapley, A. E., Pettini, M., Steidel, C. C., Reddy, N. A., & Adelberger, K. L. 2006a, *ApJ*, 644, 813
- Erb, D. K., Steidel, C. C., Shapley, A. E., Pettini, M., Reddy, N. A., & Adelberger, K. L. 2006b, *ApJ*, 646, 107

- Fazio, G. G., Hora, J. L., Allen, L. E., Ashby, M. L. N., Barmby, P., Deutsch, L. K., Huang, J.-S., Kleiner, S., Marengo, M., Megeath, S. T., Melnick, G. J., Pahre, M. A., Patten, B. M., Polizotti, J., Smith, H. A., Taylor, R. S., Wang, Z., Willner, S. P., Hoffmann, W. F., Pipher, J. L., Forrest, W. J., McMurty, C. W., McCreight, C. R., McKelvey, M. E., McMurray, R. E., Koch, D. G., Moseley, S. H., Arendt, R. G., Mentzell, J. E., Marx, C. T., Losch, P., Mayman, P., Eichhorn, W., Krebs, D., Jhabvala, M., Gezari, D. Y., Fixsen, D. J., Flores, J., Shakoorzadeh, K., Jungo, R., Hakun, C., Workman, L., Karpati, G., Kichak, R., Whitley, R., Mann, S., Tollestrup, E. V., Eisenhardt, P., Stern, D., Gorjian, V., Bhattacharya, B., Carey, S., Nelson, B. O., Glaccum, W. J., Lacy, M., Lowrance, P. J., Laine, S., Reach, W. T., Stauffer, J. A., Surace, J. A., Wilson, G., Wright, E. L., Hoffman, A., Domingo, G., & Cohen, M. 2004, *ApJS*, 154, 10
- Feigelson, E. D., & Nelson, P. I. 1985, *ApJ*, 293, 192
- Finkelstein, S. L., Rhoads, J. E., Malhotra, S., & Grogin, N. 2009, *ApJ*, 691, 465
- Gawiser, E., Francke, H., Lai, K., Schawinski, K., Gronwall, C., Ciardullo, R., Quadri, R., Orsi, A., Barrientos, L. F., Blanc, G. A., Fazio, G., Feldmeier, J. J., Huang, J.-s., Infante, L., Lira, P., Padilla, N., Taylor, E. N., Treister, E., Urry, C. M., van Dokkum, P. G., & Virani, S. N. 2007, *ApJ*, 671, 278
- Gawiser, E., van Dokkum, P. G., Gronwall, C., Ciardullo, R., Blanc, G. A., Castander, F. J., Feldmeier, J., Francke, H., Franx, M., Habertzettl, L., Herrera, D., Hickey, T., Infante, L., Lira, P., Maza, J., Quadri, R., Richardson, A., Schawinski, K., Schirmer, M., Taylor, E. N., Treister, E., Urry, C. M., & Virani, S. N. 2006, *ApJ*, 642, L13
- Giavalisco, M., & Dickinson, M. 2001, *ApJ*, 550, 177
- Giavalisco, M., Ferguson, H. C., Koekemoer, A. M., Dickinson, M., Alexander, D. M., Bauer, F. E., Bergeron, J., Biagetti, C., Brandt, W. N., Casertano, S., Cesarsky, C., Chatzichristou, E., Conselice, C., Cristiani, S., Da Costa, L., Dahlen, T., de Mello, D., Eisenhardt, P., Erben, T., Fall, S. M., Fassnacht, C., Fosbury, R., Fruchter, A., Gardner, J. P., Grogin, N., Hook, R. N., Hornschemeier, A. E., Idzi, R., Jogee, S., Kretchmer, C., Laidler, V., Lee, K. S., Livio, M., Lucas, R., Madau, P., Mobasher, B., Moustakas, L. A., Nonino, M., Padovani, P., Papovich, C., Park, Y., Ravindranath, S., Renzini, A., Richardson, M., Riess, A., Rosati, P., Schirmer, M., Schreier, E., Somerville, R. S., Spinrad, H., Stern, D., Stiavelli, M., Strolger, L., Urry, C. M., Vandame, B., Williams, R., & Wolf, C. 2004, *ApJ*, 600, L93
- Giavalisco, M., Steidel, C. C., & Macchetto, F. D. 1996, *ApJ*, 470, 189
- Granato, G. L., Lacey, C. G., Silva, L., Bressan, A., Baugh, C. M., Cole, S., & Frenk, C. S. 2000, *ApJ*, 542, 710
- Gronwall, C., Ciardullo, R., Hickey, T., Gawiser, E., Feldmeier, J. J., van Dokkum, P. G., Urry, C. M., Herrera, D., Lehmer, B. D., Infante, L., Orsi, A., Marchesini, D., Blanc, G. A., Francke, H., Lira, P., & Treister, E. 2007, *ApJ*, 667, 79
- Hainline, K. N., Shapley, A. E., Kornei, K. A., Pettini, M., Buckley-Geer, E., Allam, S. S., & Tucker, D. L. 2009, *ApJ*, 701, 52
- Hansen, M., & Oh, S. P. 2006, *MNRAS*, 367, 979
- Hayashino, T., Matsuda, Y., Tamura, H., Yamauchi, R., Yamada, T., Ajiki, M., Fujita, S., Murayama, T., Nagao, T., Ohta, K., Okamura, S., Ouchi, M., Shimasaku, K., Shioya, Y., & Taniguchi, Y. 2004, *AJ*, 128, 2073
- Hu, E. M., & McMahon, R. G. 1996, *Nature*, 382, 231
- Isobe, T., & Feigelson, E. D. 1990, in *Bulletin of the American Astronomical Society*, Vol. 22, *Bulletin of the American Astronomical Society*, 917–918
- Isobe, T., Feigelson, E. D., & Nelson, P. I. 1986, *ApJ*, 306, 490
- Iye, M., Ota, K., Kashikawa, N., Furusawa, H., Hashimoto, T., Hattori, T., Matsuda, Y., Morokuma, T., Ouchi, M., & Shimasaku, K. 2006, *Nature*, 443, 186
- Kennicutt, R. C. 1998, *ARA&A*, 36, 189
- Lai, K., Huang, J.-S., Fazio, G., Gawiser, E., Ciardullo, R., Damen, M., Franx, M., Gronwall, C., Labbe, I., Magdis, G., & van Dokkum, P. 2008, *ApJ*, 674, 70
- Lavalley, M. P., Isobe, T., & Feigelson, E. D. 1992, in *Bulletin of the American Astronomical Society*, Vol. 24, *Bulletin of the American Astronomical Society*, 839–840
- Lee, K.-S., Giavalisco, M., Gnedin, O. Y., Somerville, R. S., Ferguson, H. C., Dickinson, M., & Ouchi, M. 2006, *ApJ*, 642, 63
- Madau, P. 1995, *ApJ*, 441, 18
- Madau, P., Ferguson, H. C., Dickinson, M. E., Giavalisco, M., Steidel, C. C., & Fruchter, A. 1996, *MNRAS*, 283, 1388
- Maiolino, R., Nagao, T., Grazian, A., Cocchia, F., Marconi, A., Mannucci, F., Cimatti, A., Pipino, A., Ballero, S., Calura, F., Chiappini, C., Fontana, A., Granato, G. L., Matteucci, F., Pastorini, G., Pentericci, L., Risaliti, G., Salvati, M., & Silva, L. 2008, *A&A*, 488, 463
- Malhotra, S., & Rhoads, J. E. 2002, *ApJ*, 565, L71
- Mas-Hesse, J. M., Kunth, D., Tenorio-Tagle, G., Leitherer, C., Terlevich, R. J., & Terlevich, E. 2003, *ApJ*, 598, 858
- Matsuda, Y., Yamada, T., Hayashino, T., Tamura, H., Yamauchi, R., Ajiki, M., Fujita, S. S., Murayama, T., Nagao, T., Ohta, K., Okamura, S., Ouchi, M., Shimasaku, K., Shioya, Y., & Taniguchi, Y. 2004, *AJ*, 128, 569
- McCarthy, J. K., Cohen, J. G., Butcher, B., Cromer, J., Croner, E., Douglas, W. R., Goeden, R. M., Grewal, T., Lu, B., Petrie, H. L., Weng, T., Weber, B., Koch, D. G., & Rodgers, J. M. 1998, in *Proc. SPIE Vol. 3355*, p. 81-92, *Optical Astronomical Instrumentation*, Sandro D'Odorico; Ed., Vol. 3355, 81–92
- McLure, R. J., Cirasuolo, M., Dunlop, J. S., Foucaud, S., & Almaini, O. 2009, *MNRAS*, 392, 528
- Neufeld, D. A. 1990, *ApJ*, 350, 216
- . 1991, *ApJ*, 370, L85
- Nilsson, K. K., Møller, P., Möller, O., Fynbo, J. P. U., Michałowski, M. J., Watson, D., Ledoux, C., Rosati, P., Pedersen, K., & Grove, L. F. 2007, *A&A*, 471, 71
- Nilsson, K. K., Möller-Nilsson, O., Möller, P., Fynbo, J. P. U., & Shapley, A. E. 2009a, in preparation
- Nilsson, K. K., Tapken, C., Moeller, P., Freudling, W., Fynbo, J. P. U., Meisenheimer, K., Laursen, P., & Oestlin, G. 2008, *ArXiv e-prints*
- Nilsson, K. K., Tapken, C., Möller, P., Freudling, W., Fynbo, J. P. U., Meisenheimer, K., Laursen, P., & Östlin, G. 2009b, *A&A*, 498, 13
- Oke, J. B., Cohen, J. G., Carr, M., Cromer, J., Dingizian, A., Harris, F. H., Labrecque, S., Lucinio, R., Schaal, W., Epps, H., & Miller, J. 1995, *PASP*, 107, 375
- Oke, J. B., & Gunn, J. E. 1983, *ApJ*, 266, 713
- Ouchi, M., Shimasaku, K., Akiyama, M., Simpson, C., Saito, T., Ueda, Y., Furusawa, H., Sekiguchi, K., Yamada, T., Kodama, T., Kashikawa, N., Okamura, S., Iye, M., Takata, T., Yoshida, M., & Yoshida, M. 2008, *ApJS*, 176, 301
- Ouchi, M., Shimasaku, K., Okamura, S., Furusawa, H., Kashikawa, N., Ota, K., Doi, M., Hamabe, M., Kimura, M., Komiyama, Y., Miyazaki, M., Miyazaki, S., Nakata, F., Sekiguchi, M., Yagi, M., & Yasuda, N. 2004, *ApJ*, 611, 685
- Papovich, C., Dickinson, M., & Ferguson, H. C. 2001, *ApJ*, 559, 620
- Pentericci, L., Grazian, A., Fontana, A., Castellano, M., Giallongo, E., Salimbeni, S., & Santini, P. 2009, *A&A*, 494, 553
- Pentericci, L., Grazian, A., Fontana, A., Salimbeni, S., Santini, P., de Santis, C., Gallozzi, S., & Giallongo, E. 2007, *A&A*, 471, 433
- Pettini, M., Kellogg, M., Steidel, C. C., Dickinson, M., Adelberger, K. L., & Giavalisco, M. 1998, *ApJ*, 508, 539
- Pettini, M., Rix, S. A., Steidel, C. C., Adelberger, K. L., Hunt, M. P., & Shapley, A. E. 2002, *ApJ*, 569, 742
- Pettini, M., Shapley, A. E., Steidel, C. C., Cuby, J.-G., Dickinson, M., Moorwood, A. F. M., Adelberger, K. L., & Giavalisco, M. 2001, *ApJ*, 554, 981
- Press, W. H., Teukolsky, S. A., Vetterling, W. T., & Flannery, B. P. 1992, *Numerical Recipes in FORTRAN: the Art of Scientific Computing* (Cambridge: University Press, 2nd ed.)
- Prévot, M. L., Lequeux, J., Prévot, L., Maurice, E., & Rocca-Volmerange, B. 1984, *A&A*, 132, 389
- Quider, A. M., Pettini, M., Shapley, A. E., & Steidel, C. C. 2009, *MNRAS*, 1081
- Reddy, N. A., & Steidel, C. C. 2009, *ApJ*, 692, 778
- Reddy, N. A., Steidel, C. C., Erb, D. K., Shapley, A. E., & Pettini, M. 2006a, *ApJ*, 653, 1004
- Reddy, N. A., Steidel, C. C., Fadda, D., Yan, L., Pettini, M., Shapley, A. E., Erb, D. K., & Adelberger, K. L. 2006b, *ApJ*, 644, 792
- Reddy, N. A., Steidel, C. C., Pettini, M., Adelberger, K. L., Shapley, A. E., Erb, D. K., & Dickinson, M. 2008, *ApJS*, 175, 48
- Renzini, A. 2006, *ARA&A*, 44, 141
- Rhoads, J. E., Malhotra, S., Dey, A., Stern, D., Spinrad, H., & Jannuzi, B. T. 2000, *ApJ*, 545, L85
- Salpeter, E. E. 1955, *ApJ*, 121, 161

- Shapley, A. E., Steidel, C. C., Adelberger, K. L., Dickinson, M., Giavalisco, M., & Pettini, M. 2001, *ApJ*, 562, 95
- Shapley, A. E., Steidel, C. C., Erb, D. K., Reddy, N. A., Adelberger, K. L., Pettini, M., Barmby, P., & Huang, J. 2005, *ApJ*, 626, 698
- Shapley, A. E., Steidel, C. C., Pettini, M., & Adelberger, K. L. 2003, *ApJ*, 588, 65
- Siana, B., Smail, I., Swinbank, A. M., Richard, J., Teplitz, H. I., Coppin, K. E. K., Ellis, R. S., Stark, D. P., Kneib, J.-P., & Edge, A. C. 2009, *ApJ*, 698, 1273
- Siana, B., Teplitz, H. I., Chary, R.-R., Colbert, J., & Frayer, D. T. 2008, *ApJ*, 689, 59
- Stanway, E. R., Bunker, A. J., Glazebrook, K., Abraham, R. G., Rhoads, J., Malhotra, S., Crampton, D., Colless, M., & Chiu, K. 2007, *MNRAS*, 376, 727
- Steidel, C. C., Adelberger, K. L., Giavalisco, M., Dickinson, M., & Pettini, M. 1999, *ApJ*, 519, 1
- Steidel, C. C., Adelberger, K. L., Shapley, A. E., Pettini, M., Dickinson, M., & Giavalisco, M. 2000, *ApJ*, 532, 170
- . 2003, *ApJ*, 592, 728
- Steidel, C. C., Giavalisco, M., Dickinson, M., & Adelberger, K. L. 1996, *AJ*, 112, 352
- Steidel, C. C., Shapley, A. E., Pettini, M., Adelberger, K. L., Erb, D. K., Reddy, N. A., & Hunt, M. P. 2004, *ApJ*, 604, 534
- Tapken, C., Appenzeller, I., Noll, S., Richling, S., Heidt, J., Meinköhn, E., & Mehlert, D. 2007, *A&A*, 467, 63
- Teplitz, H. I., McLean, I. S., Becklin, E. E., Figer, D. F., Gilbert, A. M., Graham, J. R., Larkin, J. E., Levenson, N. A., & Wilcox, M. K. 2000, *ApJ*, 533, L65
- Vanzella, E., Giavalisco, M., Dickinson, M., Cristiani, S., Nonino, M., Kuntschner, H., Popesso, P., Rosati, P., Renzini, A., Stern, D., Cesarsky, C., Ferguson, H. C., & Fosbury, R. A. E. 2009, *ApJ*, 695, 1163
- Verhamme, A., Schaerer, D., Atek, H., & Tapken, C. 2008, *A&A*, 491, 89
- Verma, A., Lehnert, M. D., Förster Schreiber, N. M., Bremer, M. N., & Douglas, L. 2007, *MNRAS*, 377, 1024
- Wilson, J. C., Eikenberry, S. S., Henderson, C. P., Hayward, T. L., Carson, J. C., Pirger, B., Barry, D. J., Brandl, B. R., Houck, J. R., Fitzgerald, G. J., & Stolberg, T. M. 2003, in *Instrument Design and Performance for Optical/Infrared Ground-based Telescopes*. Edited by Iye, Masanori; Moorwood, Alan F. M. *Proceedings of the SPIE*, Volume 4841, 451–458
- Witt, A. N., & Gordon, K. D. 2000, *ApJ*, 528, 799